**Title**
Investigating Meningeal Dissemination in B-Cell Acute Lymphoblastic Leukemia



**Author**
Ho, Emily Elizabeth

**Publication Date**
2016

Peer reviewed|Thesis/dissertation

# Investigating Meningeal Dissemination in B-Cell Acute Lymphoblastic Leukemia

by

Emily Elizabeth Ho

A dissertation submitted in partial satisfaction of the

requirements for the degree of

Doctor of Philosophy

in

Molecular and Cell Biology

in the

Graduate Division

of the

University of California, Berkeley

Committee in charge:
Professor Lin He, Chair
Professor David H. Raulet
Professor Astar Winoto
Professor Martyn Smith
Professor Mary Nakamura

Summer 2016

Abstract

Investigating Meningeal Dissemination in a Model of B-cell Acute Lymphoblastic Leukemia

by

Emily Elizabeth Ho

Doctor of Philosophy in Molecular and Cell Biology

University of California, Berkeley

Professor Lin He, Chair

Leptomeningeal dissemination (LMD) is frequently observed in patients with B-cell acute lymphoblastic leukemia (B-ALL), particularly those that carry the Philadelphia chromosome ($Ph^+$). To prevent disease relapse from B-ALL cells in the meninges, patients are treated prophylactically with intrathecal chemotherapy, which is often accompanied by deleterious side effects such as neuropathy. Using a mouse model of B-ALL that recapitulates the genetic lesions commonly found in $Ph^+$ B-ALL (expression of Ph and loss of tumor suppressor *Arf*), I characterized the molecular and cellular defects during meningeal dissemination, and explored the underlying mechanism through which B-ALL cells promote meningeal dissemination. In this $Ph^+$ B-ALL model, meningeal dissemination was found in conjunction with extensive osteoclast-mediated osteolysis in the skull, caused by the expansion and activation of osteoclasts. Repression of osteoclast differentiation and activation in the Ph+ B-ALL model, either by RANK-Fc or bisphosphonate treatment, significantly delayed the onset of meningeal dissemination, suggesting the osteolysis of the skull provides a favorable stromal environment for meningeal tumor growth. I also found that the $Ph^+$ B-ALL tumors exhibited a high level of *Rankl* and *Tnfα,* at least in part, through aberrant STAT5A signaling downstream of inappropriate activation of the ABL kinase component of the BCR-ABL fusion protein. *Rankl* and *Tnfα* both promote osteoclast differentiation and osteolysis, and hence, early colonization and expansion of $Ph^+$ B-ALL cells in the meninges. Taken together, my studies reveal an unexpected connection between meningeal dissemination and osteolysis, and will likely provide important insights into patient stratification and LMD prevention in human B-ALL patients.

**Table of Contents**

**List of Figures and Tables**

**List of Abbreviations**

AF10 – ALL1-Fused Gene From Chromosome 10 Protein
AF4 – ALL1-Fused Gene From Chromosome 4 Protein
AF6 – ALL1-Fused Gene From Chromosome 6 Protein
AF9 – ALL1-Fused Gene From Chromosome 9 Protein
ALL – Acute Lymphoblastic Leukemia
AML1 – Acute Myeloid Leukemia 1 Protein
AP – Alkaline Phosphatase
B-ALL – B-cell Acute Lymphoblastic Leukemia
BCR – Breakpoint Cluster Region
BL – Burkitt Lymphoma
BMP – Bone Morphogenetic Protein
c-ABL – ABL proto-oncogene 1, non-receptor tyrosine kinase
CBL – Casitas B-Lineage Lymphoma Proto-Oncogene
CCRK – cyclin-dependent kinase 20
CDKN2A – Cyclin Dependent Kinase Inhibitor 2A
CM – Carcinomatous Meningitis
CNS – Central Nervous System
CRKL – CRK Like Proto-oncogene, adaptor protein
CSF – Central Nervous System
CTGF – Connective Tissue Growth Factor
CXCL12 – C-X-C Motif Chemokine Ligand 12
CXCR4 – C-X-C Motif Chemokine Receptor 4
DKK1 – Dickkofp1
E2A – Transcription Factor 3
EBF1 – Early B-Cell Factor 1
ENL – Myeloid/Lymphoid Or Mixed-Lineage Leukemia; Translocated To, 1
ERAS – ES Cell Expressed Ras
FGF – Fibroblast Growth Factor
GAB2 – GRB2 Associated Binding Protein 2
GRB2 – Growth Factor Receptor Binding Protein 2
HCK – Hematopoietic Cell Kinase
HL – Hodgkin Lymphoma
IGF – Insulin-like Growth Factor
IKAROS – IKAROS Family Zinc Finger 1
IL-11 – Interleukin-11
IL-15 – Interleukin-15
IL-1 – Interleukin-1
LHX1 – LIM Homeobox 1
LM – Leukemic Meningitis
LMD – Leptomeningeal Dissemination
m-CSF – Macrophage Colony Stimulating Factor
MDSC – Myeloid Derived Suppressor Cells
MIP-1a – Macrophage Inflammatory Protein 1$\alpha$
MIP-1b – Macrophage Inflammatory Protein 1$\beta$
MLL – Myeloid/Lymphoid Or Mixed-Lineage Leukemia Protein 1

MM – Multiple Myeloma
MMP – Matrix Metalloproteinase
NHL – Non-Hodgkin Lymphoma
OB – Osteoblast
OC – Osteoclast
OCP – Osteoclast Precursor
OPG – Osteoprotegerin
OPN – Osteopontin
PAX5 – Paired Box 5
PBMC – Peripheral Blood Mononuclear Cell
PBX1 – Pre-B-Cell Leukemia Homeobox 1
Ph – Philadelphia Chromosome
PTH – Parathyroid Hormone
PTHrP – Parathyroid Hormone Related Protein
PXN – Paxillin
RANK – Receptor Activator Of NF-KB
RANKL – Receptor Activator Of Nuclear Factor Kappa B Ligand
RB1 – Retinoblastoma 1
SFRP – Secreted Frizzled Related Protein
SHH – Sonic Hedgehog
SOS – Son Of Sevenless Homolog 1
STAT – Signal Transducer And Activator Of Transcription
T-ALL – T-cell Acute Lymphoblastic Leukemia
TEL – ETS Variant 6
TGFβ – Transforming Growth Factor β
TNFα – Tumor Necrosis Factor α
TP53 – Tumor Protein 53

**Acknowledgements**

My graduate work has been a constant surprise and challenge and I would like to thank all of the people who have made this thesis possible.

First and foremost, I want to thank Lin for her willingness to allow me to explore a project that was outside the lab's expertise. My passion for this project was inspired by the unique biology and the associated challenges. Thank you for finding the resources and people to support and guide this project. Lin, thank you for letting me follow the science where it (and I) wandered.

I also want to thank my thesis committee, David Raulet, Astar Winoto, Martyn Smith, and Mary Nakamura, for all of their support and scientific input.

To the He Lab, past and present, thank you for the fun times and the good science. In particular, I'd like to thank the fantastic undergraduates who have helped with my research and taught me about mentoring. Byron, thank you for your unfailing enthusiasm and passion for science, all the hard work and many hours of sectioning. Paper towel rolls will always make me think of you. Leah, thank you for your dedication and helping me get the B-ALL project up and running. And finally, thank you especially to Max, who has not only been an asset on the bench, but also stepped up to pick up the slack and keep my experiments running through both my surgery and my thesis.

I would also like to thank my friends, in particular Jenn and Shreya. Jenn, thank you for being my work wife and partner in crime. We have come so far and I couldn't have done it without you! Thank you for taking care of me, helping me to pick up the slack and always having my back. I would never have made it through my Ph. D. without your support, understanding, and scientific feedback. Shreya, thank you for all of your support in science and in life. Thank you for challenging me, always telling me the truth, and holding me accountable. Thank you for your wisdom.

Brayden, thank you for always being there for me, good times and bad. Thank you for always making sure I am well-fed and wearing clean clothes, and for always finding a way to make me laugh. Thank you for supporting me and encouraging me in my research and my thesis and for never getting mad when I'm running late. Thank you for your understanding.

Finally, I would like to thank my parents and my brother for all of their support and understanding throughout not just my time at UC Berkeley, but throughout all of my academic training. I would not be where I am without your time and effort, your advice, or your support. Thank you for your understanding when my science kept me from coming home for the holidays and for flying me home when I could. Especially, I want to my mom for all the scientific discussions and being my sounding board. Thank you, mom, for sending me papers, supporting me emotionally, and for taking care of me after my surgery. I couldn't have done this without you. Thank you for all of your support through all of my decisions.

# Chapter 1
# Introduction

Dissemination and Metastasis

It is estimated that in the United States, approximately 1.7 million people will be diagnosed with cancer and 600,000 people will die from their tumors in 2016.[1] Although there have been great advances in cancer prevention, early monitoring, detection technology, surgery techniques and treatment options, very few of these malignancies can be cured. Importantly, most terminally ill patients do not succumb to their primary tumor, but instead to metastatic disease.[2]

Metastatic lesions are the result of the dissemination of tumor cells from the primary tumor to distant tissues throughout the body, where the tumor cells proliferate to form new tumors. The process of metastasis is highly inefficient, as there are many abilities that a tumor cell must acquire to survive to form a metastatic lesion. In order to successfully metastasize, a cell must leave the primary tumor, intravasate into a nearby blood or lymph vessel, survive in circulation, extravasate out of the blood or lymph vessel into a new tissue, colonize the new tissue to form micro-metastases, and then undergo expansion into macro-metastasis or metastatic lesions. In 1889, Stephen Paget proposed the "seed and soil" hypothesis, which posited that the seeds (the disseminating tumor cells) would only grow in the soil (the tissue microenvironment) that was appropriate for their growth.[3] This hypothesis was based on the observation that in 735 necropsies of breast cancer patients, he found metastasis in certain tissues (e.g., liver and bone) at higher rates, suggesting a preference for these tissues and giving rise to the idea of tissue tropism.

The idea of cancer metastasis tissue tropism has endured and grown since Paget's time. Modern imaging techniques coupled with increased survival time resulted in enhanced observation that has allowed for better characterization of cancer metastasis tissue tropism. For example, we now know that breast cancer most commonly metastasizes to the liver and bone, as Paget observed, but also to the brain and the lung.[4] Metastatic tropism has also been observed in many other different types of cancer, such as bone metastasis in prostate cancer.[4] These observations have allowed researchers to begin to unravel the molecular mechanism underlying tissue tropism. For example, Kang *et al.* demonstrated that expression of Interleukin-11 (*IL11*), Osteopontin (*OPN*), with either Connective Tissue Growth Factor (*CTGF*) or C-X-C Motif Chemokine Receptor 4 (*CXCR4*) promotes bone metastasis in a xenograft model of human breast cancer cells in mice.[5] Interestingly, the mechanism of bone metastasis depends on the tumor type, as prostate cancer bone metastasis is associated with Endothelin-1 (*ET-1*) expression.[6] Metastatic tissue tropism can also be affected by the ease of access due to anatomical proximity. For example, colorectal cancer metastasizes to the liver with high frequency, which is thought to be due to draining of cancer cells from the colon, through the portal vein to the liver.[4] Although the tissue specificity and mechanism may vary from cancer type to cancer type, many types of cancer display tissue tropism during metastasis.

As metastasis is frequently the cause of death for most cancer patients, it is critical to illuminate the biology underlying the process of metastasis and the tissue tropism of different cancers. This knowledge will allow for better design and development of treatments to inhibit or prevent metastasis, leading to fewer cancer related deaths. Given the wide variety in types of cancer, sites of metastasis, and mechanisms of tissue tropism, it is unlikely that a single therapy will be applicable to all cancers. Thus, it is essential to have a comprehensive understanding of the tissue tropism and metastatic ability of each individual type of cancer.

Central Nervous System Metastasis – Leptomeningeal Dissemination

Among the many tissues to which cancer cells can metastasize, the central nervous system (CNS) is one of the most devastating for patient quality of life and most challenging to therapeutically access. Both solid and hematopoietic malignancies can disseminate from the primary tumor to the CNS, which is comprised of the brain parenchyma, the spinal cord, and the cranial and spinal meninges. In the cranium, the brain parenchyma is encased in the meninges and the skull (Figure 1). The meninges consist of three layers called the dura mater, the arachnoid mater, and the pia mater. The dura mater is a thick, hard layer directly adjacent to the skull that contains sinuses for the drainage of cerebral spinal fluid (CSF).[7,8] The dura mater connects the skull to the leptomeninges, which consists of the arachnoid mater, the subarachnoid space, and the pia mater.[9] The arachnoid mater and subarachnoid space are named for the resemblance of the trabeculae in the subarachnoid space to spider webs. The subarachnoid space contains CSF, which functions to cushion the brain parenchyma from mechanical forces, and blood vessels.[10] Together, the CSF and blood vessels provide nutrients and waste removal for the brain. The pia mater is the final layer of the meninges that lies directly on the brain parenchyma and plays a role in mediating the blood brain barrier, as it has been shown to allow diffusion of some small molecules from the subarachnoid space to the brain while preventing the entry of larger molecules and regulating cell entry.[7,9,11] The functions of the meninges described here also apply to the spinal cord, although subtle differences exist and are extensively reviewed by Nicolas and Weller.[12]

Infiltration into the parenchyma and the meningeal layers, or both, is observed in human patients. Solid tumors more frequently invade the parenchyma and hematopoietic tumors predominately disseminate to the meninges.[13–17] It is estimated that ~25% of all cancer patients will have metastatic disease in the CNS at some point in the course of their disease, although CNS metastasis is most commonly observed in later stage cancers.[13] Given the critical importance for patients to maintain a functional CNS and the limited treatment available for treating metastasis in the CNS, patients with metastasis to the CNS generally have extremely poor prognoses. Furthermore, in both solid and hematopoietic malignancies, CNS metastasis has increased in frequency, compared to historical controls. It is thought that the increase is due several developments: (1) improved screening to detect CNS infiltration, (2) extended patient survival due to improved therapy, and (3) poor penetration of therapy across the blood brain barrier (BBB), which creates a therapy-privileged sanctuary for residual disease.[14,18]

CNS metastasis can be generally categorized as either brain (parenchyma) metastasis or leptomeningeal dissemination (LMD). Parenchymal metastasis is most common in solid tumors, particularly in lung cancer, which represents 40-50% of all brain metastasis, and breast cancer, which accounts for 10-30% of brain parenchyma metastasis.[14,17] Hematopoietic cancers, for example Non-Hodgkin Lymphoma (NHL), can metastasize to the brain parenchyma, although usually in concurrence with LMD.[19] LMD is most commonly diagnosed in patients with primary brain tumors, hematopoietic cancers, and some solid tumors. Patients with primary brain tumors, such as medulloblastoma, have a higher risk for LMD (30-50%), particularly in conjunction with initial diagnosis, rather than during relapse.[18,20] The majority of patients with solid tumors and hematopoietic malignancies who develop LMD do so after treatment of the primary tumor. It is estimated that only 3-20% of patients with solid tumors will develop LMD, while LMD will be found in 10-70% of patients with hematopoietic malignancies, depending on the type of cancer

and method of inspection.[18,19,21,22] Given the high frequency of LMD, identification of the mechanisms driving cancer cells to metastasize to the meninges is essential for the design of better prophylactic treatments and therapies.

LMD specifically refers to dissemination to either the pia or arachnoid layers of the meninges and can occur in either or both of the cranial and spinal meninges. When solid tumors metastasize to the meninges, it is called carcinomatous meningitis (CM). Solid tumors rarely present with CM at time of diagnosis, but roughly 3-8% of patients develop CM during the course of their disease.[18] The frequency of CM is likely under represented, as it is not routinely screened for and autopsies have revealed as many as 20% of patients with CM.[22] The most common solid tumors to infiltrate the meninges are breast (12-50%), lung (10-26%), or melanoma (5-25%).[18,22] Given the poor prognosis and severe reduction in quality of life associated with CM, it may be beneficial to increase screening for meningeal metastases before symptoms arise.

Alternatively, it is currently estimated that 5-15% of patients with hematopoietic cancer will develop metastatic lesions in the meninges, known as leukemic meningitis (LM).[16,19] The frequency of LM has been dramatically reduced with prophylactic intrathecal chemotherapy. Importantly, patients with Acute Lymphoblastic Leukemia (ALL), a group that includes B-cell (B-ALL) and T-cell ALL (T-ALL) and Burkitt Lymphoma (BL), would have LM at the time of relapse in as many as 50-75% of patients if not for the addition of prophylactic intrathecal chemotherapy to standard treatment protocols, reducing LM relapse to 5-10%.[18,23] Other hematopoietic malignancies that have increased risk for LM are acute myelomonocytic leukemia (20%) and NHL (5-10%).[18,19] Nevertheless, regardless of frequency, all patients with LMD have an extremely poor prognosis due to the poor efficacy of treatment and negative effects of treatment on patient quality of life. A better understanding of the mechanism underlying LMD may allow for more targeted, and therefore less toxic, treatments for meningeal metastasis.

Although there are many published articles about LMD, the vast majority of these papers are clinical in nature and refer only to clinical observations, treatment strategies, the frequency of LMD, or correlations between LMD and different clinical parameters, such as age, gender, and response to initial treatments. Although many patients develop LMD during the course of their cancer, there are very few treatments options available, all with dramatic side effects that disrupt the function of the nervous system. Unfortunately, there is a great dearth of knowledge with regards to the mechanism by which tumor cells are able to seed the leptomeninges and wreak havoc in the CNS, unchecked and inaccessible to medical intervention. As our knowledge of the mechanism underlying LMD progresses, we will improve our ability to develop therapeutic strategies to prevent and treat LMD with fewer side effects, preserving patient quality of life.

Mechanism of Carcinomatous Meningitis

In solid tumors, the mechanism of the formation of CM is poorly characterized, as studies have primarily focused on clinical treatment strategies.[21,22,24,25] Studies of the mechanism of CM are likely hindered by the lack of tractable *in vivo* animal models.[26] Nevertheless, CM is generally thought to occur through: (1) local invasion from a primary CNS tumor, (2) extravasation through microscopic blood vessels in the meninges, (3) invasion along the cranial or spinal nerves, or (4) invasion from the cervical lymph nodes.[21,22,24,27] Studies have suggested that an

increase in the ability to migrate, adhere to endothelial cells for intravasation, and survive in the new microenvironment, will promote formation of CM.[13] However, these are more general traits of metastasis and knowledge about the mechanisms that lead specifically to CM are undefined for the majority of solid tumors. One notable exception is CM in medulloblastoma, a primary CNS tumor predominantly found in pediatric patients. CM in medulloblastoma is the best studied LMD in solid tumors due to the high frequency, as it is estimated ~50% of medulloblastoma patients will have CM, and the availability of murine mouse models.[18,26] It is believed that tumor cells infiltrate from the primary tumor in the cerebellum to the CSF, which circulates in the meninges, allowing the medulloblastoma cells to infiltrate the meninges. To better understand the mechanism of medulloblastoma metastasis in the meninges, studies have used transposon screens to identify genes that promote dissemination of medulloblastoma cells to the meninges, such as ES Cell Expressed Ras (*Eras*), Lim Homeobox 1 (*Lhx1*), and Cyclin-Dependent Kinase 20 (*Ccrk*).[28,29] Further mechanistic studies are needed to better elucidate the mechanisms of carcinomatous meningitis in different solid tumor types.

Mechanism of Leukemic Meningitis

In hematopoietic cancers, the mechanism underlying LMD is still being defined. The majority of studies have focused on LMD in ALL, which is the hematopoietic cancer with the highest frequency of LMD. ALL can be categorized as either T-cell or B-cell ALL, both of which are associated with infiltration of the CNS. Many studies have begun to piece together the mechanism that drives dissemination to the meninges in T-ALL. For example, researchers have shown that Notch-driven T-ALL uses C-C Motif Chemokine Receptor 7 (CCR7) signaling to infiltrate the CNS, both in mouse models and in xenografts of patient samples.[30] However, in a more recent study, Jost *et al*. demonstrated that CXCR4 was essential for LMD formation in mouse and human T-ALL cells and, in contrast with the previous study, that CCR7 was dispensable, perhaps due to the differences in their animal models.[31] Thus, even in one type of cancer, there is disagreement about the mechanism for LMD formation and further study is required.

The mechanism driving LMD in B-ALL is still incomplete, even though there are more cases of B-ALL LMD and more published studies, than in T-ALL. Most recently, Williams *et al*. proposed that the ability to infiltrate the meningeal layer was a general ability that the vast majority of primary human precursor-B-cell ALL tumor cells possessed, regardless of previously assigned CNS risk.[32] Furthermore, they propose that the formation of LMD was likely to be dependent upon the ability of the B-ALL cells ability to survive and proliferate in the new meningeal microenvironment.[32] Given these observations, the distinction between B-ALL cells that can and cannot form LMD may be defined by their ability to respond to tumor-derived or stromal-derived support factors in the meningeal layers.

Unfortunately, there are few studies that address the mechanism behind B-ALL infiltration of the CNS and meningeal layers. However, these studies support the supposition that the B-ALL cells' ability to interact with the meningeal microenvironment. B-ALL-derived IL-15, which is correlated with ALL infiltration of the CNS, has been shown to support *in vitro* proliferation under low serum conditions, which the authors compared to low protein CSF.[33,34] In addition, human stromal cell types found in the meningeal microenvironment have been shown to attract, interact, and protect ALL cells from chemotherapy-induced apoptosis.[35] However, all the studies

to date have demonstrated correlations between supportive factors and meningeal dissemination without illustrating a requirement *in vivo* for those factors. Moving forward, if all B-ALL cells are able to infiltrate the CNS, but not all can flourish there, patient stratification and prophylactic inhibition of LMD demands a better definition of the mechanism underlying the ability of ALL cells to commandeer the meningeal layer.

Murine models of leptomeningeal dissemination

Leptomeningeal dissemination was described as early as 1870,[20,21] but the development of *in vivo* animal models to study LMD remains ongoing. Animal models have been established in mice, rats, rabbits, and guinea pigs to study LMD.[26] Historically, the primary function for many of these animal models was to test the efficacy of systemic and intrathecal chemotherapy or other treatments in development, such as immunotherapy, as it is thought that the leptomeninges may serve as a therapy privileged area. Unfortunately, the majority of existing LMD models present challenging technical complications, such as injection of tumor cells directly into the CSF or carotid artery, to ensure engraftment of tumor cells in the meninges. Furthermore, such methods of seeding tumor cells eliminate the possibility of studying the biological mechanisms of early trafficking and engraftment in the meninges. Animal models that can recapitulate the spontaneous dissemination of tumor cells to the meninges allow for the best modeling of the early steps in LMD.

Classically, to model LMD arising from primary brain tumors, the principal models use glioma or medulloblastoma cells. Two well characterized rat glioma cell lines, C6 and 9L, have historically been used to study the efficacy of chemotherapy, immunotherapies, and gene transfer therapies on glioma LMD, using syngeneic transplantation of these tumors directly into the CSF or intracarotid injection to seed the leptomeninges.[26] Researchers have also been able to xenograft human glioma cells in immune-compromised mice and rats and test chemotherapy combinations, immunotherapies, and MRI conditions.[26,36] Medulloblastoma cells are also used to model primary brain tumor LMD, historically, by human xenografts.[26] More recently, spontaneous genetic mouse models have been developed, using activation of the Sonic Hedgehog (SHH) pathway. Expression of constitutively active Smoothened in granule neuron precursors induced medulloblastomas with high frequency of LMD.[37] Researchers have also identified genes that may play a role in LMD by using the Sleeping Beauty transposon to screen on sensitized genetic backgrounds.[29,38,39] These spontaneous models of medulloblastoma LMD are essential, as they allow researchers to dissect the signaling necessary for dissemination to the meninges.

LMD from solid carcinomas is primarily modeled in animals through intrathecal or intracarotid injection of syngeneic or allograft cells. Rat and mouse syngeneic models have been used to study underlying biology, such as immune cell involvement, as well as chemotherapy efficacy.[26] The rabbit VX2 carcinoma syngeneic model has been used for MRI studies and chemotherapy testing.[25,26,40] Finally, human solid tumor cells can be xenografted into immune-compromised rats and mice to study intrathecal immunotherapies.[26,41] For example, human melanoma lines were xenografted by intracarotid injection in immune compromised mice, giving rise to LMD.[42] While these models are optimal for testing therapeutic options on established LMD, spontaneous animal models with meningeal metastasis of carcinoma cells are rare and limit efforts to understand the pathophysiology of carcinomatous meningitis development.

As leukemic meningitis is more common in human patients, researchers have been driven to develop more models of LMD in hematopoietic malignancies. This is aided by the ease of orthotopically transplanting lymphoma and leukemia cells, which can then spontaneously disseminate to the meninges. Both genetic mouse models and xenograft models using patient leukemia or lymphoma cells have been described.[26,30–32,43,44] Historically, researchers used mouse, rat, and guinea pig syngeneic models to test chemotherapy efficacy, immunotherapies, and underlying biology.[26] More recently, with a better understanding of the genetic alterations that drive specific leukemias and lymphomas, researchers have been able to create genetic mouse models, specifically both transplantation and spontaneous, to model LMD for different leukemias and lymphomas.[30,32,34,45,46] Combined with xenograft of primary human patient tumor cells, these models have allowed researchers to delve deeper into the components that are critical for LMD (and CNS). For example, Buonamici *et al*. identified that CCR7 signaling is critical in both a transplantation and spontaneous mouse model of Notch-induced T-cell acute lymphoblastic leukemia (T-ALL).[30] They were further able to demonstrate that CCR7 signaling was also critical for human T-ALL cells homing to the CNS in a xenograft model, thereby validating the necessity for animal models to investigate the mechanisms underlying meningeal dissemination.[30] Recent studies examining LMD in B-ALL have suggested that while trafficking to the meninges may be a common ability,[32] formation of symptom inducing LMD may depend on the ability of the B-ALL cells to survive and thrive in that environment.[34,35] These studies emphasize the need for animal models that recapitulate the spontaneous meningeal dissemination to interrogate the mechanism of early colonization and expansion of tumor cells in the meninges. In particular, this is essential for B-ALL if all B-ALL cells can traffic to the meninges but not all can thrive to become LMD.

Cancers of the Hematopoietic System

Cancers of the hematopoietic cancers account for 10% of all cancers.[1,47] Hematopoietic malignancies are defined by their common lineage that traces back to the hematopoietic stem cell, although the mechanism of tumorigenesis and disease presentation and progression varies between subtypes. The three main subtypes of hematopoietic cancers are leukemia, lymphoma, and myeloma, which are characterized based on the anatomical location of the malignancy and the specific cell type that gives rise to the disease. Leukemia is classically defined as a malignancy of the blood, normally with neoplastic white blood cells accounting for an aberrantly large fraction of the total blood volume. Leukemia predominately arises in the bone marrow from an inappropriate outgrowth of transformed myeloid or lymphoid cells, followed by entrance into blood circulation and continued proliferation. In the United States, leukemia is the most common form of pediatric cancer, accounting for 30% of all pediatric oncology cases, and the seventh most fatal cancer in adult patients.[1] Classically, leukemia is categorized by cell lineage (myeloid or lymphoid) and progression rate (quickly, referred to as acute, or more slowly, referred to as chronic). Thus, the four major subtypes are Acute Myelogenous Leukemia (AML), Chronic Myelogenous Leukemia (CML), Acute Lymphoblastic Leukemia (ALL) and Chronic Lymphoblastic Leukemia (CLL). Together, these subtypes account for ~90% of all leukemia. Lymphoma differs from leukemia primarily in the anatomical location of the abnormal cells. Although they can both arise in the bone marrow, lymphoma cells form solid masses instead of remaining in blood circulation. Furthermore, lymphoma originates only from the lymphoid lineage, which includes B-cell, T-cell, and NK-cells. Approximately 90% of lymphomas are categorized as non-Hodgkin lymphoma (NHL), which are the most aggressive lymphomas and

the eighth most fatal cancer-type in the United States.[1,48] The remaining 10% of lymphomas are Hodgkin lymphomas (HL), which are one of the least common and least fatal cancers in the United States.[1] Finally, although myeloma is not as common as leukemia or lymphoma, but it is the 15th most commonly diagnosed cancer in 2016.[1] Myeloma is derived from aberrantly proliferating plasma cells, usually found in bone marrow throughout the bones of the body, and commonly associated with debilitating bone degradation.[48] Although hematopoietic malignancies share a common lineage, LMD is predominately observed in patients with leukemia. Thus, the focus of LMD research in hematopoietic cancers should focus on probing meningeal dissemination in leukemia models.

B-cell Acute Lymphoblastic Leukemia

Of the four major subtypes of leukemia, ALL is the most common form of pediatric cancer, representing 20-25% of all pediatric cancer, the majority of which are of the B-cell lineage.[47–50] In the pediatric B-ALL patients, cure rates are very promising after prophylaxis for CNS infiltration, nearing 80-90%.[50,51] Although not as common in adults, patients with ALL over the age of 20 have much poorer prognosis, with only 30-40% of patients attaining long term remission.[50,52] In both pediatric and adult ALL, the majority of patients are diagnosed with B-ALL, with only 10-15% of children and 20-25% of adults presenting with T-ALL.[50,52] The majority of B-ALL malignancies are considered precursor B-ALL, as the tumor cells do not express IgM, a membrane bound form of immunoglobulin specific to mature B-cells. A small subset of the B-ALL, roughly 1-5%, express IgM, classifying these leukemias as mature B-cell ALLs, which includes Burkitt Lymphoma (BL).[50] Although the category of B-ALL includes these mature B-cell malignancies, from here on B-ALL will refer specifically to precursor B-cell ALLs. Given the strong proclivity for B-ALL cells to disseminate to the meninges, further characterization of the mechanism underlying LMD formation in B-ALL is essential to develop prophylactic treatments less toxic than intrathecal chemotherapy.

Genetic Alterations in B-cell Acute Lymphoblastic Leukemia

B-ALL can be further subcategorized by different genetic alterations, each with different prognoses and expected event free survival (EFS). One important distinction is between B-ALL with hyperdiploidy (>50 chromosomes) and hypodiploidy (<44 chromosomes), the former of which is both more prevalent and associated with better prognosis than the latter.[53] Mutations and/or deletions of several gene categories have also been observed in B-ALL patients, most commonly in genes associated with disrupting the normal B-cell developmental program (Paired Box 5 (*PAX5*), IKAROS Family Zinc Finger 1 (*IKZF1*), and Early B-Cell Factor 1 (*EBF1*)), inhibition of tumor suppressor genes (including Tumor Protein P53 (*TP53*), Cyclin-Dependent Kinase Inhibitor 2a (*CDKN2A*), and Retinoblastoma 1(*RB1*)) and activation of members of other well studied proliferation signaling pathways (Ras, tyrosine kinase, and cytokine receptor signaling).[50,53,54] However, the majority of the characterized genetic changes in B-ALL are aberrant translocations between two non-homologous proteins, resulting in abnormal fusion proteins. These translocations can affect a myriad of anomalous changes, such as inappropriate activation of signaling pathways, by creating chimeric transcription factors with impaired or excessive transcriptional activity.

Some of the most common translocations that result in chimeric transcription factors include t(1;19)(q23;p13), known as *E2A-PBX1*, t(12;21), known as *TEL-AML1*, and a variety of

translocations involving *MLL*. These three families of translocations result in unique chimeric proteins with aberrant transcription factor function. *E2A-PBX1* translocations are found in 25% of pediatric B-ALLs and associated with poor prognosis under the standard therapy regimen.[50,54] Juxtapositioning of Transcription Factor 3 (*E2A*), a transcription factor critical for normal B-cell development, and Pre-B-Cell Leukemia Homeobox 1 (*PBX1*), a transcription factor that normally regulates the HOX transcription pathway, has been shown to induce transformation in *in vitro* assays[50,54,55] and in *in vivo* mouse models.[56] *E2A-PBX1* is thought to promote leukemia through deregulation of normal E2A function and aberrant transcriptional activity of the novel fusion protein.[50,54–56] *TEL-AML1* translocations are more common in pediatric B-ALL (30%) than adult B-ALL (1-3%) and associated with a favorable outcome for pediatric patients.[50,54] This translocation combines the oligomerization and repression functions of ETS Variant 6 (*TEL*, normally an ETS transcription factor) and the DNA binding activity of Acute Myeloid Leukemia 1 Protein (*AML1*, normally involved in regulating DNA binding of the core-binding factor to regulate hematopoiesis) to result in binding of *AML1* target genes and aberrant repression of these genes by DNA methylation.[50,54,57] Finally, Myeloid/Lymphoid Or Mixed-Lineage Leukemia Protein 1 (*MLL*) is associated with a wide variety of different translocations (] 50-70 different translocations have been reported),[49,50] which are extremely common in infant patients with ALL (85%), but less common in adult patients (3-8%)[50,54] The most common of the *MLL* translocations include ALL1-Fused Gene From Chromosome 4 Protein (*AF4*), ALL1-Fused Gene From Chromosome 6 Protein (*AF6*), ALL1-Fused Gene From Chromosome 9 Protein (*AF9*), ALL1-Fused Gene From Chromosome 10 Protein (*AF10*), and Mixed-Lineage Leukemia; Translocated to, 1 (*ENL*), which account for approximately 80% of the whole family of translocations.[50] MLL is normally involved in promoting expression of members of the HOX family of transcription factors.[50,58] The MLL translocations all include the N-terminal end of the MLL protein and the C-terminal end of the fusion partner; studies have shown the chimeric protein aberrantly activates MLL signaling, and can result in leukemia as a result of increased self renewal of hematopoietic progenitor cells.[49,50,58–60] Thus, these commonly observed translocations contribute to B-ALL tumorigenicity through aberrant transcriptional activity.

One of the most well characterized translocation is t(9;22)(q34;q11), also known as the Philadelphia chromosome (Ph), which results in the chimeric BCR-ABL fusion protein. First described as the predominant driving genetic lesion in CML, *BCR-ABL* is also expressed in 3-5% of pediatric and 30% of adult of B-ALL ($Ph^+$ B-ALL).[50,52,54] Patients with $Ph^+$ B-ALL have extremely poor prognoses and are at higher risk for CNS infiltration and relapse.[50,52,54,61–63] Of the three isoforms of the BCR-ABL fusion protein, the most common form in $Ph^+$ B-ALL is $p190^{BCR\text{-}ABL}$. The fusion of BCR and ABL proteins preserves the tyrosine kinase activity of ABL kinase and the dimerization domains of BCR, resulting in an aberrantly dimerized and activated ABL kinase activity.[64–67] The constitutively active fusion kinase activates downstream signaling pathways such as Ras, Akt/PI3K, and STAT signaling that lead to increased proliferation.[64–67]

The Philadelphia Chromosome: BCR-ABL

The Philadelphia chromosome (Ph), also known as t(9;22)(q34;q11) and the *BCR-ABL* gene, was initially described in 1960, when technology was developed that allowed visualization of chromosomes.[65] *BCR-ABL* is the driving genetic lesion in 90% of all CML patients and is present in a subset of B-ALL patients ($Ph^+$ B-ALL, 3-5% of pediatric patients, 30% of adult patients).[50,52,64,67,68] The *BCR-ABL* fusion gene is created by a reciprocal translocation that

juxtapositions the 5' end of the Breakpoint Cluster Region (*BCR*) with the 3' end of the ABL proto-oncogene 1, non-receptor tyrosine kinase (*c-ABL*) (Figure 2).[64–67]

There are three regions in *BCR* that give rise to different break points with different amounts of *BCR* fused with *c-ABL*, resulting in different isoforms of *BCR-ABL*. All the isoforms contain the same region of *c-ABL*, starting in exon 2. The most common break point in *BCR* has been named major break point (M-bcr) and contains exons 13 and 14. Thus, this creates the junctions e13a2 and e14a2 and the fusion protein $p210^{BCR\text{-}ABL}$ (Figure 2).[65,67] This isoform of BCR-ABL is the most common and present in 99% of CML patients and 33% of $Ph^+$ B-ALL patients.[67] The second most common isoform of BCR-ABL is $p190^{BCR\text{-}ABL}$, which is present in the majority of $Ph^+$ B-ALL patients. $p190^{BCR\text{-}ABL}$ is formed by translocation at the minor break point (m-bcr) in BCR at exon 1, creating junction e1a2 (Figure 2). Finally, use of a third break point in BCR at exon 19 gives rise to a rare isoform of BCR-ABL known as $p230^{BCR\text{-}ABL}$ (Figure 2).

All three isoforms of BCR-ABL possess the ability to induce CML-like disease by overexpression in mouse models through the constitutively active kinase activity of the fusion protein.[67,69] The BCR portion of the fusion protein contains coiled-coil protein domains that promote dimerization or oligomerization of the fusion protein.[64,66,70] The dimerization of BCR-ABL proteins facilitates autophosphorylation events, especially at the SH2 and SH3 domains from c-ABL, which leads to increased recruitment of downstream signaling proteins and increased signaling.[66,67,70] Under physiological conditions, c-ABL's subcellular location oscillates between the cytoplasm and the nucleus; BCR-ABL is retained in the cytoplasm, despite a nuclear localization signal, which also contributes to its ability to aberrantly interact with and drive signaling pathways.[66,67] For example, BCR-ABL autophosphorylation results in increased recruitment of Growth Factor Receptor Bound Protein 2 (GRB2), GRB2 Associated Binding Protein 2 (GAB2), and Son Of Sevenless Homolog 1 (SOS), which activates the RAS pathway.[66–68,70] RAS activation leads to downstream activation of both the MAPK and AKT/PI3K signaling pathways, which leads to increase proliferation and decreased apoptosis.[67,70] BCR-ABL is also known to increase STAT signaling directly and indirectly by phosphorylation of Signal Transducer And Activator of Transcription (STAT) 1 and 5, and Hematopoietic Cell Kinase (HCK), respectively.[66,67,70] BCR-ABL is also known to affect actin cytoskeletal function through interactions with the RAC GTPases and downstream signaling molecules such as CRK Like Proto-oncogene, adaptor protein (CRKL), Casitas B-Lineage Lymphoma Proto-Oncogene (CBL), Paxillin (PXN), and other actin interacting proteins.[66,68,70]

Although all three isoforms of BCR-ABL have similar abilities in CML, $p190^{BCR\text{-}ABL}$ preferentially induces B-cell acute lymphoblastic leukemia in mice over the other isoforms.[69] Thus, in mouse models of $Ph^+$ B-ALL, the $p190^{BCR\text{-}ABL}$ isoform is primarily chosen to drive leukemogenesis.[44,45,71] Furthermore, disruption of the tumor suppressor *CDKN2A/B* (from here, known as *ARF*) function in patients with $Ph^+$ B-ALL has been frequently reported, with some reports as high as 64% of patients.[72,73] It has been shown that expression of *BCR-ABL* in mouse B-cells induces the Arf protein and promotes apoptosis,[45] explaining the high frequency of observed loss of *ARF* in human patients. Together, these two genetic lesions give rise to a highly clinically relevant, reproducible, and genetically tractable system for studying B-ALL, as described by Williams *et al*.[45] This model of $Ph^+$ *Arf*$^{-/-}$ B-ALL has been used for a wide variety of

studies, including studying cooperating genetic lesions[74,75] and the response and resistance to Ph specific inhibitors.[44,76–78]

Bone Homeostasis

Bone homeostasis is a tightly regulated process to ensure the proper balance between bone degradation and bone formation. Under normal physiological conditions, the balance between these two states may shift to favor either degradation or formation of bone, but the process for one is tightly coupled to the other so that homeostasis is maintained. To connect the process of bone degradation and formation, osteoclasts (OCs) and osteoblasts (OBs), the two cell types directly responsible for bone degradation and formation, respectively, and other cell types in the bone microenvironment communicate and regulate the function and differentiation of OCs and OBs (Figure 3). Other cells in the bone microenvironment that contribute to bone homeostasis are osteocytes, bone lining cells, osteomacs, and B- and T-cells.[79]

OCs are large, multi-nucleated cells, derived from the hematopoietic lineage, that function to secrete proteolytic enzymes and to create localized acidic environments to break down bone.[79,80] OCs use their actin cytoskeleton to form tight seals between the OCs and the surface of the bone, creating resorption lacunae into which the OCs secrete acid and proteinases and from which the OCs absorbs growth factors and other degradation products released from the bone, to release into the micronenvironment.[81] OCs are differentiated from osteoclast precursors (OCPs), which are mononucleated myeloid/monocyte/macrophage progenitor cells, although the exact molecular marker definition of the OCP is not conclusively defined.[79,80,82] It has been well established that OCs can be derived from OCPs found in whole bone marrow, which is the primary source for OCPs for *in vitro* differentiation studies with mouse cells, and in the peripheral blood, from which peripheral blood mononuclear cells (PBMCs) are harvested for studying human OC differentiation *in vitro*. Other studies have reported unique subsets of myeloid/monocytic cells may be able to serve as OCPs, as demonstrated by a population of myeloid derived suppressor cells (MDSCs) differentiating into OCs in a mouse model of rheumatoid arthritis.[83] Regardless of the source, OCPs require Macrophage Colony Stimulating Factor (m-CSF), for proliferation and survival, and Receptor for Activation of Nuclear Factor Kappa B Ligand (RANKL) to drive differentiation and fusion of OCPs into mature, bone resorbing OCs. RANKL has been shown to be the most essential factor for OC differentiation, both in *in vitro* differentiation assays and *in vivo,* as *Rankl*$^{-/-}$ mice fail to form OCs and are osteopetrotic.[84] Binding of RANKL to its cognate receptor Receptor Activator Of NF-κB (RANK) on the surface of OCPs drives a specific gene expression program driven by Nuclear Factor Kappa B (*NFκB*).[79] m-CSF is predominantly secreted by OBs and other stromal cell types; RANKL is thought to be expressed by OBs, osteocytes, vascular endothelial cells, and T-cells.[79] OB may also secrete osteoprotegerin (OPG), which is a soluble secreted decoy receptor for RANKL and serves to inhibit differentiation of OC.[79,81,85] Nevertheless, in pathological conditions, m-CSF and/or RANKL may be secreted aberrantly to drive abnormal OC activity (to be discussed in later sections).

OBs are the lone cells directly mineralizing and forming bone. There are two types of bone formation: intramembranous and endochondral ossification, which are defined by the different tissue that is mineralized to form the bone. Intramembranous ossification occurs when connective tissue, formed primarily from collagen, is ossified, primarily in flat bones (such as the

skull and shoulder blades). Endochondral ossification occurs when previously formed cartilage is gradually ossified and replaced with bone, such as the elongation of the long bones (such as the tibia and fibia).[79] OBs are the cell type that is responsible for the mineralization in both intramembranous and endochondral ossification. OBs are derived from the mesenchymal stem cell lineage and directly differentiate from preosteoblasts, which, although they do express alkaline phosphatase (AP), are not able to mineralize bone.[79] Differentiation of OBs is highly dependent upon Wnt signaling and expression of Wnt inhibitors (such as Dickkopf-1 (DKK-1) and Secreted Frizzled Related Protein (sFRP)) will inhibit OB differentiation, and therefore, function. Transforming Growth Factor β (TGFβ) and Bone Morphogenetic Protein (BMP) signaling can also drive recruitment and differentiation of OBs, and serve as mechanism to couple bone degradation and formation, as TGFβ and BMP are stored in the bone matrix and released by osteoclast mediated bone degradation.[79,81] Likewise, OBs serve to positively regulate OC activity through expression of *m-Csf* and *Rankl*. OB expression of these factors can also be induced in the microenvironment by factors such as Parathyroid Hormone Related Protein (PTHrP), Tumor Necrosis Factor α (TNFα), Interleukin-1 (IL-1) and 1,25-$(OH)_2$ vitamin $D_3$.[79,85] OBs can also positively and negatively regulate OCPs. OBs express chemoattractants, some of which are embedded in the bone matrix and only released upon OC activity, which recruit OCPs to the local site of bone remodeling and increase OC numbers. Alternatively, OBs also negatively regulate OCs through secretion of OPG to inhibit OC differentiation from OCPs. Finally, after bone formation is complete at a given site, the majority of OBs will apoptose, while some terminally differentiate into osteocytes or bone lining cells. Thus, OBs are not only critical for bone formation, but also for tightly controlling OC activity.

Both osteocytes and bone lining cells are terminally differentiated from OB and function to contribute to OC and OB regulation.[79,86,87] Osteocytes are embedded within lamellar bone and are thought to contribute to regulating OCs and OBs, as well functioning as a sensor for mechanical strain on the bone.[79,88] In response to hormones, such as Parathyroid Hormone (PTH) and mechanical stress, osteocytes down regulate Sclerostin, which normally functions to inhibit OB activity; thus, in the presence of PTH or mechanical stress, osteocytes function to activate OB mediate bone formation.[88] This is consistent with the observation that increased mechanical stress in the form of exercise can lead to increased bone mass, while decreased loading of the bones leads to bone loss (i.e. space related bone loss). Moreover, in the absence of mechanical stress, osteocyte apoptosis is induced, which stimulates OC activity and bone loss.[88] Osteocytes can also directly secrete RANKL or OPG to regulate OC differentiation.[88] Bone lining cells are also terminally differentiated OBs, although less well characterized as osteocytes. It has been suggested that during the early stages of bone degradation, the bone lining cells are revealed and migrate to form a "canopy," which serves to keep the local area of remodeling (and secreted factors) contained to support the coupling of the OC and OB activities.[79,87] Furthermore, it has also been suggested that the bone lining cells may support OCP differentiation in the local environment through expression of membrane bound RANKL, inducing only local differentiation.[87] Therefore, both osteocytes and bone lining cells contribute to regulating the balance between OCs and OBs.

Osteomacs are a population of resident macrophages in the bone that function to positively regulate bone mineralization.[79] Although macrophages have been observed as a part of the bone microenvironment, Chang *et al.* coined the term "osteomac" and demonstrated that these resident

macrophages support the OB population and function.[89] Furthermore, Chang *et al.* were able to remove the osteomacs *in vivo* and demonstrate a loss of bone mass, consistent with an imbalance in bone homeostasis favoring osteoclast activity and the observed loss of osteoblasts. [89] Interestingly, these studies suggest that the osteomacs may not serve as a pool of OCPs, as there was not a concurrent reduction in OC activity.[90]

T- and B-cells have also been shown to play a role in bone homeostasis. Under normal physiological conditions, studies suggest that both T-cells and B-cells function to inhibit osteoclastogenesis.[79] T-cell inhibition of osteoclast differentiation was demonstrated *in vitro* and *in vivo*: depletion of T-cells ($CD4^+$ and $CD8^+$) from mouse bone marrow enhanced osteoclastogenesis and mice depleted of T-cells also displayed a higher level of osteoclast activity as evidenced by their decrease bone mass.[79] However, under inflammatory conditions, such as those found in arthritis, activated T-cells are induced to secrete RANKL, which acts to stimulate osteoclastogenesis and bone loss.[79,91,92] Similarly, B-cells have been shown to inhibit osteoclast differentiation *in vivo*, as B-cell deficient mice have decreased bone mass. This decrease in bone mass is proposed to be the result of increased osteoclast activity due to the loss of B-cell secreted OPG.[79] As T-cells have been shown to support B-cell secretion of OPG, it is likely that decreased levels of OPG in T-cell deficient mice contribute to their loss of bone mass.[79] As in T-cells, activation of B-cells in an inflammatory context can induce *Rankl* expression, which can support osteoclastogenesis.[91]

Osteolysis in Cancer

Under pathological conditions, the balance between bone formation and bone degradation can be skewed, resulting in aberrant bone loss or aberrant bone growth. Such imbalance in bone homeostasis can occur when cancer cells metastasize to the bone. Metastatic lesions that result in bone loss are called osteolytic lesions, while those that cause bone formation are called osteoblastic lesions. As stated earlier, certain cancer types show preferential metastatic potential for bone, most commonly breast and prostate carcinomas. Multiple myeloma (MM) is a hematopoietic malignancy of plasma cells and commonly resides in the bone marrow; although these are not classified as bone metastases, MM is commonly associated with osteolysis and will also be summarized here.

Breast cancer cells frequently metastasize to the bone and it is estimated that 50-70% of breast cancer patients will have bone metastasis at autopsy.[93,94] In breast cancer, although some bone metastases are characterized as osteoblastic (bone forming) lesions, the vast majority of breast cancer bone metastasis are diagnosed as osteolytic lesions, characterized by bone loss around the breast cancer cells. These lesions begin the "vicious cycle," wherein the breast cancer cells drive osteoclast differentiation, resulting in growth factor release from the bone matrix, which supports the breast cancer cell proliferation and survival.[93,95] Specifically, breast cancer cells have been shown to secrete PTHrP, which drives increased expression of *Rankl* and decreased expression of *Opg* in the bone microenvironment, resulting in the differentiation and activation of osteoclasts.[95,96] The active bone degradation caused by osteoclasts releases matrix bound growth factors, such as TGFβ, fibroblast growth factors (FGFs), insulin-like growth factors (IGFs), and BMPs, which function to support the growth and survival of the colonizing breast cancer cells.[93,95,97–99] Breast cancer cells may also secrete TGFβ, which can induce the local environment to produce factors known to promote osteoclast differentiation.[100] Thus, the most

essential aspect of the breast cancer cells' induction of osteolysis is the ability to shift the balance of bone homeostasis in favor of osteoclast activation.

Prostate cancer also frequently metastasizes to the bone, with as many as 70-80% of patients with metastasis developing bone metastasis.[99–101] Although the majority of these patients have osteoblastic lesions, rather than osteolytic, a portion of prostate cancer bone metastasis contains osteolytic lesions. Studies have shown that prostate cancer cells can promote osteolysis through a variety of different mechanisms than breast cancer cells. For example, prostate cancer secreted RANKL can directly stimulate osteoclast precursors to differentiate into mature osteoclasts.[101,102] Other studies have suggested that increased levels of DKK1 may promote the osteolytic environment by shifting the balance away from osteoblast activity.[103] Prostate cancer cells may also promote an osteolytic environment through the expression of matrix metalloproteinases (MMPs), such as MMP9, which promote osteoclast activity.[103] Again, as in breast cancer, the ability to form osteolytic metastasis depends upon the ability of the prostate cancer cells to shift the balance by either enhancing osteoclast activity or decreasing osteoblast activity.

Finally, multiple myeloma (MM) is a hematopoietic malignancy of plasma cells that arises in the bone marrow and is frequently accompanied by extensive osteolysis.[104–106] It is estimated that at least 85% of MM patients present with osteolytic lesions, as opposed to breast and prostate cancers which generally develop later during metastatic disease.[104,106] Furthermore, the effects of MM on bone have been characterized as a purely lytic, with no traces of new bone growth. Thus, the balance between osteoclast and osteoblast activity is unequivocally shifted towards osteoclast activity. MM cells cause this shift by both enhancing osteoclasts and inhibiting osteoblasts. To promote osteoclast activity, not only do MM cells express *Rankl*, they also actively decrease levels of OPG in the microenvironment through two mechanisms: suppression of *Opg* expression and active encapsulation of OPG.[104,106–109] MM cells also secrete Macrophage Inflammatory Protein 1α and 1β (MIP-1α and MIP-1β), and C-X-C Motif Chemokine Ligand 12 (CXCL12), which all promote osteoclast activity through recruitment of osteoclast precursors and driving osteoclast differentiation.[104,106] Finally, like prostate cancer cells, MM cells inhibit osteoblast activity to further drive the environment towards osteolysis through expression of DKK-1 and sFRP-2, both of which inhibit Wnt signaling and suppress osteoblast differentiation and activity.[104,106] Thus, the osteolysis associated with MM depends on the ability to shift bone homeostasis to favor osteoclast activity.

Summary

Across all cancer types, human patients predominately succumb to metastatic tumor disease, rather than their primary tumors. Of all the sites of metastasis, the CNS remains one of the most fatal locations for disseminated tumor cells, as it represents one of the most challenging tissues to treat and improper CNS function can be fatal. Thus, patients with CNS metastasis are faced with extremely poor prognoses and treatments are often palliative, rather than curative. Primary brain tumors, carcinomas, and hematopoietic malignancies metastasize to the CNS, but leukemic dissemination to the meninges is one of the most frequently observed CNS metastases. Of all leukemia subtypes, B-ALL patients are at such great risk for LMD that prophylactic intrathecal chemotherapy is the gold standard treatment. Unfortunately, although this prophylaxis has decreased LMD frequencies, bathing the CNS in toxic chemotherapy often results in neuropathies that decrease patient quality of life. As the mechanism that controls leukemia

dissemination to the meninges is undefined, we are unable to develop more targeted therapies to prevent LMD formation in B-ALL patients. Thus, deeper understanding of the biology that drives LMD is essential to better stratify patients and create prophylactic treatments with fewer negative side effects.

B-ALL patients may have a variety of different genetic aberrations, but expression of the Philadelphia chromosome is associated with particularly poor prognosis due to high rates of relapse in the meninges. Previous research suggests that B-ALL cells may thrive in the meninges due to their interaction with local microenvironment. Other cancer subtypes have been shown to manipulate bone homeostasis to promote their own survival and proliferation through increasing osteoclast activity. We propose here that $Ph^+$ B-ALL may be predisposed to meningeal dissemination through aberrant activation of osteoclast activity. It appears that abnormally elevated ABL kinase activity from the fusion protein BCR-ABL inappropriately activates Stat5a signaling, which promotes expression of *Rankl* and *Tnfα* and aberrant osteoclast differentiation and activity. Thus, osteoclast activation driven by BCR-ABL in $Ph^+$ B-ALL patients may enrich the meningeal microenvironment to support B-ALL dissemination.

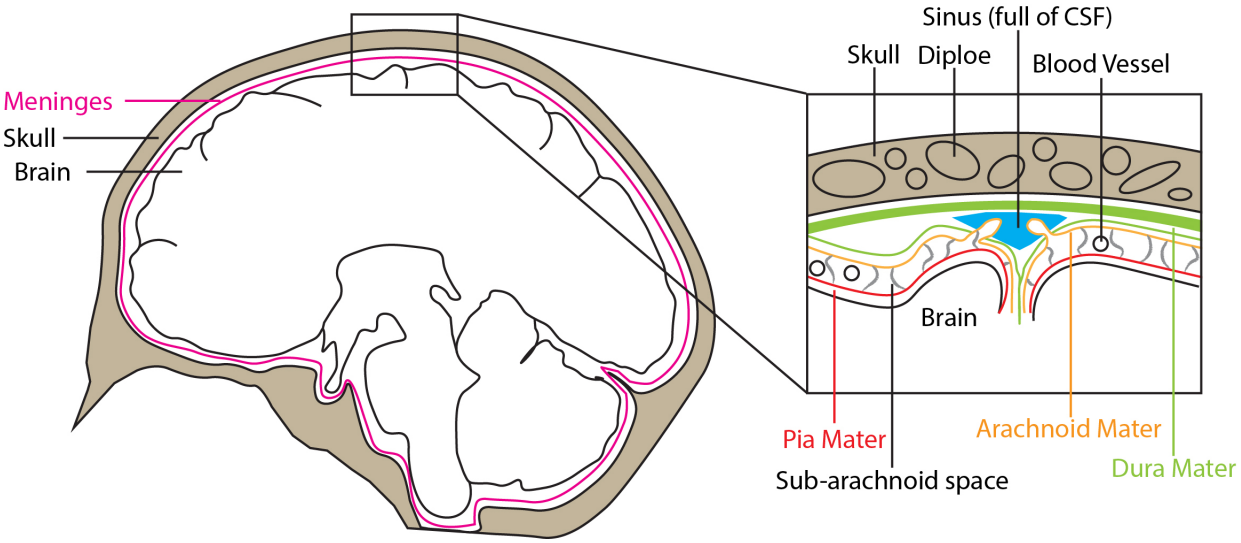


**Figure 1. Cranial Meningeal Anatomy.** In the cranium, the brain parenchyma (white) is encased in the meninges (pink) and the skull (tan). In a closer view (inset), the skull bone contains pockets of bone marrow called diploë. Underneath the skull, the meninges are made of three layers called the dura mater (green), the arachnoid mater (orange) and the pia mater (red). CSF contained in the sub-arachnoid space can drain through the arachnoid mater into the sinuses (blue triangle) found in the dura mater.

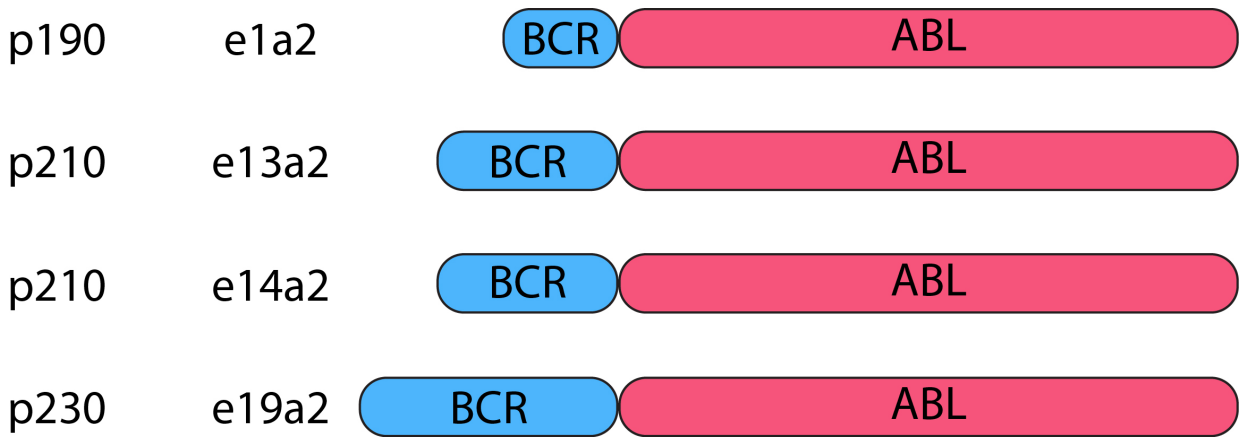


**Figure 2. Isoforms of *BCR-ABL*.** *BCR-ABL* is found in three isoforms: p190, p210, and p230. They are formed through translocation between different breakpoints in *BCR* (blue) and the same region of *ABL* (pink). The isoforms can be distinguished by the location of the break point at different exons in BCR: exon 1 (e1), exon 13 (e13), exon 14 (e14), and exon 19 (e19). This results in four different translocations that give rise to the three protein isoforms. The p190 isoform is most commonly found in Philadelphia chromosome B-cell acute lymphoblastic leukemia (and will be used in all experiments described here). The p210 and p230 isoforms are most commonly found in chronic myelogenous leukemia (CML).

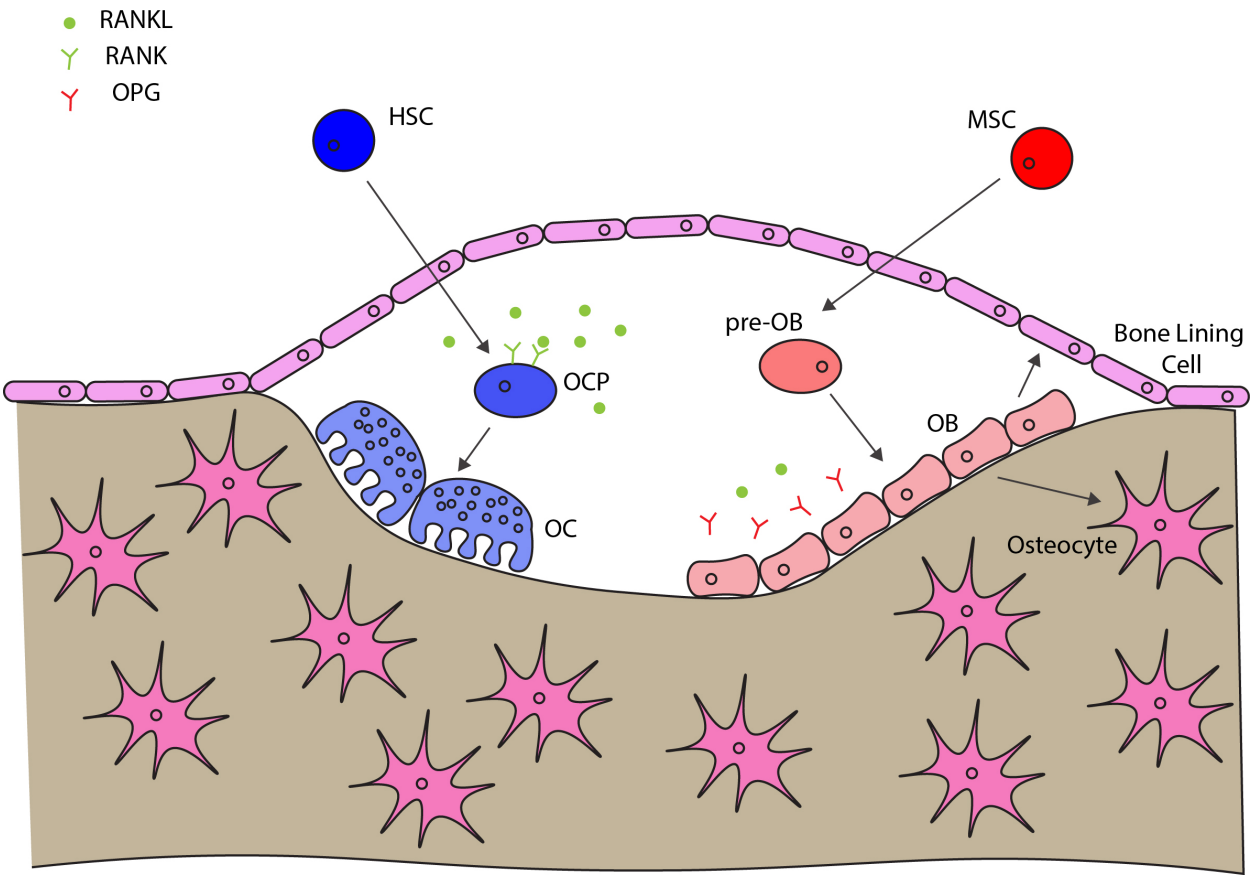


**Figure 3. Bone homeostasis is balance between bone degradation and formation.** Bone degradation is mediated by osteoclasts (OC, light blue). Osteoclasts are derived from the hematopoietic stem cell (HSC, dark blue) lineage, immediately differentiated from monocytic/myeloid osteoclast precursor cells (OCP, medium blue). This differentiation process is primarily driven by *RANKL* (green circles) binding to cognate receptor *RANK* (green Y shape) on the surface of OCP. OC mediated bone degradation results in the release of factors stored in the bone matrix, such as IGFs, FGFs, TGFβ, and BMPs. Bone formation is mediated by osteoblasts (OB, light red). Osteoblasts are derived from the mesenchymal stem cell (MSC, dark red) lineage, immediate differentiated from pre-osteoblasts (pre-OB, medium red). Osteoblasts may terminally differentiate into either bone lining cells (pale pink) or osteocytes (bright pink). Osteoblasts regulate osteoclast differentiation through secretion of *RANKL* and a soluble decoy receptor for *RANKL, OPG* (red Y shape). Osteocytes may also serve as a source for *RANKL*. Thus, the balance between bone degradation and formation is tightly regulated and coupled: OBs regulate bone degradation through *RANKL* and *OPG* expression to control OC differentiation, while OCs regulate bone formation by releasing factors, such as TGFβ from the bone to promote OB differentiation and activation.

# Chapter 2
# Methodology

Molecular cloning

The top ranking 21-bp sense sequences targeting *Rankl*, *Stat1*, *Stat3*, *Stat5a*, *Stat5b*, and *Tnf-α* were selected from the Genome Perturbation Platform (Broad Institute) as listed in Table 1. Gene specific oligos synthesized (Invitrogen) with pLKO.1 specific flanking sequence (forward oligo 5' CCGG – sense – CTCGAG – antisense – TTTTTG 3' and reverse oligo 5' AATTCAAAAA – sense – CTCGAG – antisense 3'). Oligos were resuspended to 20μM and annealed in NEB Buffer 2 by a 5 minute melt at 95˚C, incubation at 70˚C for 10 minutes, and cool down of 0.2˚C/sec until the thermocycler reached 10˚C. Annealed oligos were cloned into AgeI/EcoRI digested pLKO.1 lentiviral vector using T4 Ligase (NEB, M0202) at 16˚C overnight. Ligated plasmid was transformed into DH5α competent cells, plated on ampicillin resistant plates, PCR colony screened for inserts (AAGAATGTGCGAGACCCAGG and CAAGGCTGTTAGAGAG ATAATTGGA), and sequence verified (UC Berkeley DNA Sequencing Facility).

shRNAs targeting *Tnf-α* were selected from the Genome-wide Sensor-Based shRNA predictions (Fellmann *et al*. 2013) and cloned as previously described.[110] Briefly, 97-mer oligos were synthesized (Invitrogen) as listed in Table 1. The 97-mers were PCR amplified (TGAACTCGAGAAGGTATATTGCTGTTGACAGTGAGCG and TCTCGAATTCTAGCCCC TTGAAGTCCGAGGCAGTAGGC) with Phusion (NEB, catalogue no. M0530S), digested EcoRI/XhoI and cloned into EcoRI/XhoI digested miR-E lentiviral vector pRRL-GFP-Puro. Colonies were screened by PCR using a sequence specific primer and MSCV 5' (CCCTTGAACCTCCTCGTTCGACC) and sequence verified (UC Berkeley DNA Sequencing Facility).

Cell culture

*Arf*$^{-/-}$ *BCR-ABL* B-cell acute lymphoblastic leukemia lines (generous gift from Dr. C. Sherr at St. Jude Children's Hospital) were maintained in RPMI 1640 (Gibco, catalogue no. 11875093) with 10% fetal bovine serum, 4mM glutamine (Gibco, catalogue no. 25030081), 1x penicillin/streptomyocin (Gibco, catalogue no. 10378016), and 55μM 2-mercaptoethanol (Sigma Aldrich, catalogue no. M3148). Cells were seeded at 0.2 x $10^6$ cells/mL and split when density reached 2-4 x $10^6$ cells/mL.

Primary murine B-cells were harvested from bone marrow from *Arf*$^{-/-}$ and wildtype 4-6 week old mice and cultured in RPMI 1640 (Gibco, catalogue no. 11875093) with 10% fetal bovine serum, 4mM glutamine (Gibco, catalogue no. 25030081), 1x penicillin/streptomyocin (Gibco, catalogue no. 10378016), and 115 μM 2-mercaptoethanol (Sigma Aldrich, catalogue no. M3148), supplemented with 2.5 ng/mL IL-7 (R&D Systems, catalogue no. 407-ML-005).

*Eμ-Myc* and *Eμ-Myc p53*$^{+/-}$ lymphoma cells were cultured on irradiated 3T3 feeder cells in 45% DMEM (Gibco, catalogue no. 11995065) 45% IMDM (Gibco, catalogue no. 12440-053) with 10% fetal bovine serum, 4mM glutamine (Gibco, catalogue no. 25030081), 1x penicillin/streptomyocin (Gibco, catalogue no. 10378016), and 50 μM 2-mercaptoethanol (Sigma Aldrich, catalogue no. M3148).

293T cells and Phoenix E cells were maintained in DMEM (Gibco, catalogue no. 11995065) with 10% fetal bovine serum, and 1x penicillin/streptomyocin (Gibco, catalogue no. 10378016).

For shRNA expression in *Arf*$^{-/-}$ *BCR-ABL* B-ALL cells, shRNA was transduced through lentiviral infection with either pLKO.1 or miR-E constructs. 293T cells were plated at 1.7 x $10^6$ cells/100 mm plate and transfected the following day with either pLKO.1 or miR-E shRNA constructs, along with lentiviral packaging plasmids using polyethylenimine (linear, MW 25000, Polysciences, Inc, catalogue no. 23966). Media was exchanged at 48 hours post-transfection to RPMI, supplemented as described. At 72 hours, lentiviral-containing supernatant was filtered through a 0.45µm filter and added to B-ALL cells in a 1:1 ratio with 4µg/mL of polybrene. Selection with puromycin at 1µg/mL was started 48-72 hours post-infection and maintained for 48 hours. RNA was collected to evaluate knockdown efficiency 48-72 hours after puromycin selection ended.

B-ALL cell transplantation

To establish B-ALL *in vivo*, 4 week old, female, non-irradiated C57BL/6 were intravenously transplanted with 0.1 x $10^6$ *Arf*$^{-/-}$ *BCR-ABL* B-ALL cells. Animals were monitored and sacrificed when displaying signs of terminal illness, which include weight loss, dehydration, decreased mobility, unkempt fur, and respiratory distress. For tumor kinetic studies, animals were sacrificed pre-terminally on days 3, 6, 9, 12, and 14 after tumor transplantation, and terminally at 17 and 20 days.

For bisphosphonate and RANK-Fc experiments, 4 week old, female non-irradiated C57BL/6 mice were pretreated for 2 weeks and then through the duration of the experiment with either bisphosphonate (5 mg/kg weekly, intravenously), RANK-Fc (10 mg/kg twice weekly, subcutaneously) or PBS (by same method and schedule as drug treated animals). At 6 weeks of age, the mice were transplanted with 0.1 x $10^6$ *Arf*$^{-/-}$ *BCR-ABL* B-ALL cells and monitored. Cohorts of mice were collected at early (11-12 days post-transplantation), middle (16 days post-transplantation) and late (20 days post-transplantation) time points.

Eµ-Myc mouse model of Burkitt Lymphoma

*p53*$^{-/-}$ male mice were crossed to *Eµ-Myc*/+ female mice to generate *Eµ-Myc p53*$^{+/-}$ offspring. Mice were genotyped for the presence of the *Eµ-Myc* transgene and for *p53* status, although *Eµ-Myc p53*$^{+/-}$ offspring were identifiable by phenotype by 21 days due to runty size. Animals were monitored and sacrificed when displaying signs of terminal illness, which include weight loss, dehydration, decreased mobility, unkempt fur, and respiratory distress. Terminal illness was generally ~50 days for *Eµ-Myc p53*$^{+/-}$ mice and 90-120 days for *Eµ-Myc p53*$^{+/+}$ mice. All mice were kept on the C57BL/6 background.

Osteoclast inhibition reagents

Pamidronate disodium pentahydrate (LKT Laboratories, catalogue no. P0049) was dissolved in PBS at 0.33 mg/mL and dosed at 5 mg/kg. RANK-Fc was a generous gift from Amgen, Inc through the Extramural Research Alliances program.

Histology

Collected tissues were fixed overnight in 10% buffered formalin (Fisher Scientific, catalogue no. SF100-4). Tissues containing bone (skulls, long bones, spines, and rib cages) were decalcified for in 10% EDTA (Fisher Scientific, catalogue no. S316-212) for 5-7 days. All tissues were embedded in paraffin (American MasterTech, catalogue no. EMPARREGCS) and sectioned into

6 μm sections onto Fisherbrand Superfrost Plus Microscope slides (Fisher Scientific, catalogue no. 12-550-15) for routine staining or TruBond 360 Adhesive Microscope slides (IHC World, catalogue no. IW-T380) for immunohistochemistry. Hematoxylin (Thermo Scientific, catalogue no. 22-050-111) and eosin (Thermo Scientific, catalogue no. 22-050-110) (H&E) staining was conducted in a Gemini AS Automated Slide Stainer (Thermo Scientific). Tissues were stained for tartrate resistant acid phosphatase (TRAP) using the Acid Phosphatase, Leukocyte (TRAP) kit (Sigma Alridch, catalogue no. 387A) and mounted in Fluoromount-G Slide Mounting Medium (Fisher Scientific, catalogue no. OB100-01) following deparaffinization in Histo-Clear (Fisher Scientific, catalogue no. 50-899-90147) and rehydration in graded alcohol. For detection of Pax5 (Santa Cruz Biotechnology, catalogue no. sc-1974), representative sections were deparaffinized and rehydrated in graded alcohol and subjected to antigen retrieval treatment with 1x Dako Target Retrieval Solution, pH 6.1 (Dako, catalogue no. S1699). Sections were treated with 3% hydrogen peroxide, blocked in 5% BSA (Sigma Aldrich, catalogue no. A7906), incubated in primary antibody (diluted in 1% BSA) overnight at 4˚C in humid chambers. Antibody binding was visualized through secondary biotin coupled antibody (Jackson ImmunoResearch, catalog no. 705-065-147), avidin-HRP (Vector Laboratories, catalogue no. PK-7100) and Diaminobenzidiene (DAB) kit brown (Invitrogen, catalogue no. 002014). Samples were counterstained in Mayer's Hematoxylin (Fisher Scientific, catalogue no. 50-318-42).

Osteoclast quantification

The number of osteoclasts was analyzed by quantifying the number of TRAP positive cells along frontal and parietal bones of the calvaria, normalizing to the length of bone analyzed on the periosteum and endosteum surfaces.

Tumor area quantification

The surface area of tumor within the diploe and meninges in the skull (along the calvaria, structures under the brain were not included) was quantified using Photoshop software (Adobe Creative Cloud) and normalized to the total surface of the brain.

mRNA analysis by real-time PCR

Cultured cells and fresh-harvested tumors were processed to a single cell suspension, spun down at 1000 rpm for 5 minutes, and lysed in TRIzol Reagent (Invitrogen, catalogue no. 15596026). RNA was extracted following the manufacturer's protocol with an additional chloroform wash and followed by an ethanol precipitation. mRNA was converted to cDNA using the iScript Advanced cDNA Synthesis Kit (Bio-Rad, catalogue no.1725038). mRNA levels were analyzed real-PCR with SYBR reagents (SsoAdvanced Universal SYBR Green Supermix, Bio-Rad) for the genes listed in Table 2.

CRISPR design and electroporation

sgRNA oligos targeting upstream or downstream of the first exon of *Rankl* were synthesized (Invitrogen) with the sequences listed in Table 3. Each individual oligo and oligo T7RevLong (AAAAAAGCACCGACTCGGTGCCACTTTTTCAAGTTGATAACGGACTAGCCTTATTTT AACTTGCTATTTCTAGCTCTAAAAC) were amplified with amplification primers T7FwdAmp (GGATCCTAATACGACTCACTATAG) and T7RevAmp (AAAAAAGCACCGA CTCGG) using Phusion (NEB, catalogue no. M0530S). sgRNAs were transcribed from the PCR product using T7 RNA polymerase (NEB, catalogue no. M0251S), treated with DNAse to

remove PCR product (NEB, catalogue no. M0303L) and purified by the MEGAclear Transcription Clean-Up Kit (Ambion, catalogue no. AM1908). Purity was checked on the BioAnalyzer (UC Berkeley Functional Genomics Laboratory). sgRNAs were pre-complexed with Cas9 protein (QB3 Macrolab, UC Berkeley) in a 1:1.5 molar ratio (final concentration of 8 μM Cas9/sgRNA complex) in the following solution: 20 mM HEPES pH 7.5 (Sigma Aldrich, catalogue no. H3375), 150 mM KCl (Sigma Aldrich, catalogue no. P9333), 1 mM MgCl (Sigma Aldrich, catalogue no. M8266), 10% glycerol (Fisher Scientific, catalogue no. BP229), and 1 mM reducing agent TCEP (*tris*(2-carboxyethyl)phosphine, Sigma Aldrich, catalogue no. C4706). The Cas9/sgRNA complex was incubated for 10 minutes at 37˚C, then electroporated into *Arf*$^{-/-}$ *BCR-ABL* B-ALL cells using programs CA-137 or CV-104 and the SF Cell Lin 4D-Nucleofector X Kit L (Lonza, catalogue no. V4XC-2024) on the Lonza 4D Nucleofector. Cells were cultured and plated for single cell clones and expanded. Editing efficiency was tested in bulk and single cell clones by PCR with following primers: RANKL ext 5' (GAGCCAGAAACCAACCACTG), RANKL ext 3' (GCAGTCCAAGCAATGACACA), RANKL int 5' (ACTAACCGACCTGTTC CCTG), and RANKL int 3' (TTGGGAAGCTTAGATGCCCA).

Proliferation assay

$0.4 \times 10^6$ cells were plated at a density of $0.2 \times 10^6$ cell/mL in RPMI, supplemented as described, per well of a 6-well plates. At 48 hours, the total number of cells per well was quantified and $0.4 \times 10^6$ cells were re-plated into a new well of a 6-well plate. Cells were counted for both shRANKL and shSCRAMBLE expressing B-ALL cells every 2 days for 8 days.

BCR-ABL overexpression

For BCR-ABL overexpression studies, primary B-cells harvested from *Arf*$^{-/-}$ or wildtype 4-6 week old mice or *Eμ-Myc* or *Eμ-Myc p53*$^{+/-}$ lymphoma cells were infected with MSCV-*BCR-ABL-IRES-GFP*. Phoenix E cells were plated at $7.9 \times 10^6$ cells/100 mm plate and transfected the following day with MSCV-*BCR-ABL-IRES-GFP* and retroviral packaging plasmid using the calcium phosphate transfection protocol as previously described. Briefly, Phoenix E cell media was changed to contain chloroquine at 25 μM. 500 μL of 2x HBS was added drop wise to an agitating mix of 16 μg of the MSCV vector, 8 μg of the helper plasmid, 62.5 μL of 2M $CaCl_2$ in sterile water, total volume 500 μL. After 5 minutes of incubation, the DNA mix was added drop wise to the plate of Phoenix E cells. Media was changed to collection media 24-48 hours after transfection and collected from 48-96 hours. For experiments with primary B-cells, except for the short-term experiment, cells were infected 2-6 times over the first 3 days of culture, cultured for another 4-5 days, then sorted for GFP positivity and collected for RNA. In the short-term primary B-cell experiment, cells were infected after 5 days of culture and sorted 48 hours after the first infection. For experiments with *Eμ-Myc* or *Eμ-Myc p53*$^{+/-}$ lymphoma cells, cells were infected 2-6 times, sorted for GFP positivity, and cultured to expand the GFP+ lymphoma cells. mRNA levels were assessed in the GFP+ subset of primary B-cells and lymphoma cells.

| shRNA | Vector | Targeting Sequence |
|---|---|---|
| shRANKL #1 | pLKO.1 | GCTGATGGTGTATGTCGTTAA |
| shRANKL #2 | pLKO.1 | ATTACCTGTACGCCAACATTT |
| shRANKL #3 | pLKO.1 | CTGATGGTGTATGTCGTTAAA |
| shRANKL #4 | pLKO.1 | ATGATAGTGTGAAGGGTTAAG |
| shTNFα #1 | pLKO.1 | CCTCCCTCTCATCAGTTCTAT |
| shTNFα #2 | pLKO.1 | CACTCAGATCATCTTCTCAAA |
| shTNFα #3 | pLKO.1 | CGATGGGTTGTACCTTGTCTA |
| shTNFα #4 | pLKO.1 | GCTATCTCATACCAGGAGAAA |
| shTNFα #5 | pLKO.1 | AGCCGATTTGCTATCTCATAC |
| shTNFα #6 | pLKO.1 | CCCTGGTATGAGCCCATATAC |
| shTNFα #7 | pLKO.1 | ACCACCATCAAGGACTCAAAT |
| shTNFα #8 | pLKO.1 | TCAATCTGCCCAAGTACTTAG |
| shTNFα #9 | miR-E | ACGGCATGGATCTCAAAGACAA |
| shTNFα #10 | miR-E | ACGGGTCATTGAGAGAAATAAA |
| shTNFα #11 | miR-E | GACAGACATGTTTTCTGTGAAA |
| shSTAT1 #1 | pLKO.1 | CCTATGAGCCCGACCCTATTA |
| shSTAT1 #2 | pLKO.1 | GGACTAGAGTGCGAGTATTTG |
| shSTAT1 #3 | pLKO.1 | ACGCCTTTGGGAAGTATTATT |
| shSTAT1 #4 | pLKO.1 | CTGTTACTTTCCCAGATATTA |
| shSTAT3 #1 | pLKO.1 | CACCATTCATTGATGCAGTTT |
| shSTAT3 #2 | pLKO.1 | CGACTTTGATTTCAACTACAA |
| shSTAT3 #3 | pLKO.1 | CGACTTTGATTTCAACTACAA |
| shSTAT5A #1 | pLKO.1 | GCCATTCACGACGCGAGATTT |
| shSTAT5A #2 | pLKO.1 | TTGACCAAGATGGCGAGTTTG |
| shSTAT5A #3 | pLKO.1 | GACGTGAGATTCAAGTCTAAC |
| shSTAT5B #1 | pLKO.1 | CCCATCGAGGTGCGACATTAT |
| shSTAT5B #2 | pLKO.1 | CGCTTCTCTTTGGAAACAATA |
| shSTAT5B #3 | pLKO.1 | CGGCCAAAGGATGAAGTATAT |

**Table 1. shRNA Targeting Sequences.**

| Gene | Forward Primer | Reverse Primer |
|---|---|---|
| *Rankl* | CATTTGCACACCTCACCATC | ATGATGCCGAAAGCAAATGT |
| *Rank* | CCAGGAGAGGCATTATGAGC | CCAGGAGAGGCATTATGAGC |
| *Opg* | AGTCCGTGAAGCAGGAGTG | CCATCTGGACATTTTTTGCAAA |
| *m-Csf* | TTCAAGCTCTTTCTGAACCGTGTA | GCCTTGTTTTGTGCCATTAAGAAG |
| *c-Fms* | CATCCACGCTGCGTGAAG | GGGATTCGGTGTCGCAATAT |
| *Tnfα* | CTGAACTTCGGGGTGATCGG | GGCTTGTCACTCGAATTTTGAGA |
| *Il-1α* | CGAAGACTACAGTTCTGCCATT | GACGTTTCAGAGGTTCTCAGAG |
| *Il-1β* | AGGCTCCGAGATGAACAACA | TTGTCGTTGCTTGGTTCTCC |
| *Il-6* | GCCAGAGTCCTTCAGAGAGATACA | GCACTAGGTTTGCCGAGTAGA |
| *Il-15* | CATCCATCTCGTGCTACTTGTG | GCCTCTGTTTTAGGGAGACCT |
| *Il-34* | GGACTCGCCTGGCTATACTG | CTGAAGCCGGTTCTTGTACTG |
| *Spp1* | TCTGATGAGACCGTCACTGC | CGCTCTTCATGTGAGAGGTG |
| *Mmp7* | TAGGCGGAGATGCTCACTTT | GAGAGTGGCCAAATTCATGG |
| *Mmp9* | AAAACCTCCAACCTCACGGA | AGGGAGAGCTGCTTCTGAAG |
| *Mmp12* | TTACACTCCGGACATGAAGC | TGTACCACCTTTGCCATCAA |
| *s-Frp2* | CTAGTAGCGACCACCTCCTG | GGTGTCTCTGTTGATGTACGT |
| *Dkk1* | CCACAGCCATTTTCCTCGAG | TCTGATGATCGGAGGCAGAC |
| *Pth* | CATCATGCTGGCAGTCTGTC | CCATTGCATCCTCTCCATGG |
| *Pthrp* | CTGGTTCAGCAGTGGAGTGT | CTTGCCCTTGTCATGCAGTA |
| *Stat1* | TCACAGTGGTTCGAGCTTCAG | GCAAACGAGACATCATAGGCA |
| *Stat3* | GAGTCTAACAACGGCAGCCT | AAGGTGATCAGGTGCAGCTC |
| *Stat5a* | GTTTGAGTCTCAGTTCAGCGT | CATGGACGATAACGACCACAG |
| *Stat5b* | ACCAGATGCAGGCCTTGTAC | GAGCTGGGTGGCCTTAATGT |
| *Bcr-Abl* | CGCATGTTCCGGGACAAAAGC | GGTCATTTTCACTGGGTCCAGC |

**Table 2. qPCR Primer Sequences**

| sgRNA | Targeting Sequence |
|---|---|
| *Rankl* upstream 1 | GGAGGCCAGCTCTCTCCACG |
| *Rankl* upstream 2 | GAGCCAATCAGCCTCCAGGA |
| *Rankl* downstream 1 | GTCTTTCTCAGAGGAAGTGGG |
| *Rankl* downstream 2 | GCTAAAGATTCAGAACCTCG |

**Table 3. *Rankl* sgRNA Sequences**

# Chapter 3
# Meningeal Dissemination in $Ph^+$ B-Cell Acute Lymphoblastic Leukemia

Introduction

In recent years, chemotherapeutic treatment of B-cell acute lymphoblastic leukemia (B-ALL) has improved the cure rate in both pediatric and adult patients, yet a key barrier to long-term survival is leukemia relapse in the central nervous system (CNS). B-ALL infiltration into the CNS often precedes bone marrow relapse and indicates extremely poor prognosis,[18] leading to a median survival time after CNS relapse only six months in affected patients.[23] As 30-75% of B-ALL patients develop CNS infiltration during the course of their disease,[23,50,111,112] standard treatment now includes prophylactic CNS-directed chemotherapy. Although prophylaxis has decreased CNS relapse to 5-10% of patients, the neuropathic side effects of intrathecal chemotherapy reduces the quality of patients' lives. A better understanding of the biological mechanism underlying CNS infiltration may inspire better patient stratification and new therapies to prevent CNS infiltration without sacrificing patient quality of life.

In hematopoietic malignancy, CNS infiltration predominantly occurs in the meninges, referred to as leptomeningeal dissemination (LMD). B-ALL patients have the highest frequency of LMD, compared to all other hematopoietic cancers.[58] Currently, the mechanisms underlying B-ALL LMD remain poorly understood. Although LMD in T-cell ALL requires CCR7 signaling for infiltration into the meninges, in B-ALL this signaling proved to be unnecessary, as primary human B-ALL cells with the ability to infiltrate the meninges had variable CCR7 levels.[30,32] While the mechanism for B-ALL meningeal infiltration remains undefined, it has been proposed that the propensity to traffic to the meninges is a general ability that the vast majority of primary human B-ALL tumor cells possess, regardless of previously assigned CNS risk.[32] However, not all of the B-ALL cells were able to expand in the meninges, suggesting that the trafficking to the meninges was not sufficient for formation of LMD.[32] The mechanism underlying the tissue tropism of B-ALL cells to the meninges is ambiguous and requires further study.

As infiltration of B-ALL cells in the meninges does not always result in LMD, expansion in the meninges may depend on the ability of the B-ALL cells to groom the meningeal microenvironment for their own needs. Previous studies have suggested that B-ALL cells can enhance or exploit aspects of the meningeal microenvironment for augmented proliferation or survival. For example, B-ALL-derived Interleukin-15 (IL-15) has been correlated with CNS infiltration by B-ALL cells.[33] IL-15 has been shown to support *in vitro* proliferation of B-ALL cells under low serum conditions, which may mimic the low protein concentrations found in cerebral spinal fluid (CSF).[34] These studies suggest that IL-15 may aid survival of B-ALL cells in the meningeal CSF. Furthermore, human stromal cell types from the meningeal microenvironment have been shown to attract (in part by CXCL12 signaling) and interact with B-ALL cells *in vitro*.[35] Meningeal stromal cells also protect B-ALL cells from chemotherapy-induced apoptosis *in vitro*, although the mechanism remains undefined. These studies imply that the meninges may provide a fertile environment for B-ALL expansion.[35] Thus, the formation of B-ALL LMD *in vivo* may rely on the ability of the B-ALL cells to flourish in the meninges through exploitation of the local microenvironment.

Interestingly, 3-5% of pediatric B-ALL patients and 25-40% of adult B-ALL patients carry the Philadelphia Chromosome ($Ph^+$),[113] characterized by reciprocal chromosomal translocation between chromosomes 9 and 22 that produces a BCR-ABL fusion protein with aberrant ABL kinase activation. Patients with the Ph translocation are at higher risk to develop CNS

infiltration, making this an informative trait to study when assessing meningeal dissemination in a putative model system. Furthermore, $Ph^+$ patients commonly acquire other genetic alterations, such as deletion of the *INK4-ARF* locus observed in 67% of $Ph^+$ patients.[61,73,114] Thus, to model $Ph^+$ B-ALL in a mouse model, $Arf^{-/-}$ bone marrow stem and progenitor cells are infected by a retroviral vector to overexpresses $p185^{BCR-ABL}$ before transplantation into syngeneic recipient mice.[45,76] This murine model recapitulates the dissemination patterns observed in human B-ALL, including LMD.[44,77,78] Furthermore, the $Ph^+$ B-ALL mouse model even mimics LMD relapse following chemotherapeutic treatment, as dasatinib treatment reduces B-ALL tumor burden, but ultimately results in LMD relapse.[44] Consequently, the $Ph^+$ B-ALL mouse model provides a promising system to examine the mechanism underlying meningeal dissemination.

$Ph^+$ B-ALL mouse model exhibits extensive meningeal dissemination

The $Ph^+$ B-ALL mouse model was developed by the Sherr lab through overexpression of $p185^{BCR-ABL}$ in $Arf^{-/-}$ pre-B-cells, followed by transplantation into recipient mice.[45] To better characterize meningeal dissemination in this model, we intravenously transplanted established $Ph^+$ B-ALL cell lines (a generous gift from the Sherr Lab) into 4-week-old syngeneic C57BL/6 mice (Figure 4A). Consistent with the rate of tumor progression reported in previous studies, animals were terminal by 21 days post-injection.[44,45,77] Intriguingly, when mice were injected with $Ph^+$ B-ALL cells carrying a luciferase reporter, *in vivo* bioluminescent imaging of terminal animals revealed the greatest tumor burden in the cranial meninges (Figure 4B). This was confirmed by histological analysis (Figure 4C, D), where the meninges were the major site of B-ALL dissemination at the terminal stage, characterized by a severe disruption of typical meningeal structures due to tumor infiltration. Although B-ALL cells infiltrated the lymph nodes, spleen, and the liver, B-ALL cells were most heavily disseminated in the cranial meninges, particularly around the meningeal blood vessel under the lambdoid suture (Figure 4C, D). The infiltration of the cranial meninges was reminiscent of LMD in human B-ALL, making the $Ph^+$ B-ALL model ideal for investigating the biology underlying meningeal dissemination.[23,58,115–118]

The marked meningeal dissemination could be caused by earlier initiation of tumor colonization or enhanced tumor expansion. To differentiate between these two hypotheses, we examined the kinetics of B-ALL dissemination to different tissues by assessing the extent of dissemination every 2-3 days after transplantation of $Ph^+$ B-ALL cells (Figure 5A). In the meninges, lymph nodes, spleen, and liver, seeding of the B-ALL cells all as early as 3 days after transplantation (Figure 5B). However, the expansion of the B-ALL cells in the cranial meninges was more rapid and extensive than in other tissues, with initial expansion in the meninges at 9-12 days post-transplantation. By the terminal stage of B-ALL dissemination, the B-ALL cells completely overwhelmed the meninges and disrupted normal tissue architecture. Alternatively, expansion of B-ALL cells in other organs was incomplete, as normal tissue structures remained, despite the presence of colonizing B-ALL cells. Thus, while B-ALL cells were efficient in disseminating into various organs in our model, the cranial meninges provided a particularly fertile environment for their continued expansion.

Meningeal dissemination is associated with osteoclast-mediated osteolysis.

To better understand the relationship between the B-ALL cells in the meninges and the local microenvironment, we characterized the effect of B-ALL cells on the surrounding tissue.

Intriguingly, meningeal dissemination was associated with pronounced osteolysis characterized by extensive bone loss, pitting of the bone surface, and areas with complete loss of bone continuity (Figure 6A). The observed osteolysis could either be caused by decreased osteoblast activity or increased osteoclast activity. Using Tartrate Resistant Acid Phosphatase (TRAP) staining to identify osteoclasts, we compared the abundance of osteoclasts in calvaria in tumor free and terminal B-ALL mice. We observed a stark increase in TRAP staining in mice with meningeal dissemination (Figure 6B), suggesting that aberrantly increased osteoclast activity caused the observed osteolysis. If the B-ALL cells stimulated the increase in osteoclast activity, we would expect a correlation between the amount of B-ALL cells and osteoclasts. Strikingly, we observed a very consistent increase in osteoclasts that correlated with tumor progression (Figure 6C-E). Furthermore, the increase in osteoclasts began at 9 days after transplantation, during early B-ALL cell expansion in the meningeal layers (Figure 5B). Together these data suggest the B-ALL cells may promote the osteoclast-mediated osteolysis of the calvarial bones.

Meningeal dissemination and associated osteolysis is observed in a second mouse model

B-ALL is one of the most common hematopoietic malignancies associated with LMD, but other leukemias and lymphomas are associated with LMD in human patients. 25-50% of patients with Burkitt Lymphoma (BL) are predicted to develop LMD in the absence of prophylactic intrathecal chemotherapy.[18,19,119–121] BL is classically modeled in mice using the well established *Eμ-Myc* BL mouse model, which is driven by expression of a transgene that places *Myc* under the transcriptional control of the Eμ immunoglobulin heavy chain enhancer, mimicking the family of translocations extremely frequently observed in human BL.[122,123] Although the original study that characterized the *Eμ-Myc* BL mouse model described tumors within the cranium,[122] these tumors have not been well characterized in the subsequent studies. We generated both *Eμ-Myc/+ p53*$^{+/+}$ and *Eμ-Myc/+ p53*$^{+/-}$ mice to investigate meningeal dissemination in a second hematopoietic malignancy. As expected, loss of a single *p53* allele accelerated lymphomagenesis dramatically shortened the survival to 33% of the *Eμ-Myc p53*$^{+/+}$ mice (~45-50 days compared to ~120 days, data not shown). Histological analysis revealed that the lymphoma tumors in the cranium could be observed as early as 2 weeks after birth in *Eμ-Myc/+ p53*$^{+/-}$ mice and histologically consistent with the LMD observed in the Ph$^{+}$ B-ALL mouse model (Figure 7A and data not shown). In addition to the accelerated lymphomagenesis, the meningeal dissemination tumor burden in *Eμ-Myc/+ p53*$^{+/-}$ mice was greater than in the *Eμ-Myc/+ p53*$^{+/+}$ mice (Figure 7B). Surprisingly, while 20% *Eμ-Myc p53*$^{+/+}$ animals did have lymphoma in the cranium at frequencies consistent with initial observations (25%),[122] cranial lymphoma was nearly 4 times as common in *Eμ-Myc/+ p53*$^{+/-}$ mice (Figure 7C).

Given the similarities between the Ph$^{+}$ B-ALL mouse model and the *Eμ-Myc* BL mouse model, we analyzed the meningeal dissemination in the *Eμ-Myc* BL mouse model for osteolysis. Surprisingly, in the same regions of the calvarial bones and diploë (Figure 8A), we observed high levels of osteolysis, marked by extensive bone pitting, thinning, and discontinuity (Figure 8B, C). Furthermore, these areas are associated with TRAP staining, indicative of increased osteoclast number and activity (data not shown). The meningeal dissemination and high levels of osteoclast activity in the *Eμ-Myc* BL mouse model was highly reminiscent of the Ph$^{+}$ B-ALL model, underscoring the importance of understanding the relationship between meningeal dissemination and osteolysis.

Osteoclast activity is required for early colonization of the meninges

To determine whether osteoclasts are required for meningeal dissemination, we inhibited osteoclast differentiation by targeting RANKL activity with RANK-Fc (Amgen, Inc). Functioning as a sponge to prevent RANKL from activating osteoclast differentiation, RANK-Fc effectively inhibits osteoclasts and osteoclast-dependent tumor formation in several models.[101,109,124] We treated 4-week-old, female C57BL/6 mice twice weekly with 10 mg/kg RANK-Fc or PBS subcutaneously for two weeks before $Ph^+$ B-ALL cell transplantation and throughout the experiment (Figure 9A). $10^5$ $Ph^+$ B-ALL cells were intravenously injected into pretreated mice and collected pre-terminally at 12 and 16 days, and at 19 days, when the PBS treated animals were terminal. Intriguingly, early B-ALL colonization and expansion in the meninges was critically dependent on osteoclast activity, with 3-fold less B-ALL meningeal dissemination in pre-terminal RANK-Fc treated mice (Figure 9B, C, E). The difference in meningeal B-ALL tumor burden decreased by the terminal stage of B-ALL, suggesting the B-ALL cells adapted to expand within the meninges in the absence of osteoclasts (Figure 9D-F). Thus, the B-ALL cells' ability to manipulate osteoclast activity makes the meninges a unique microenvironment for expansion of B-ALL cells.

Osteoclast activity, not RANKL, is required for meningeal colonization

As RANKL has been shown to drive the proliferation of B-cells, it is possible that RANK-Fc treatment inhibited meningeal dissemination by decreasing B-ALL proliferation.[125,126] To eliminate this possibility, we inhibited osteoclast activity by a separate mechanism using the bisphosphonate pamidronate, which selectively inhibits osteoclast activity and causes osteoclast apoptosis.[127] As before, we pretreated recipient mice with weekly intravenous doses of 5 mg/kg pamidronate or PBS and continued to treat through the duration of the experiment (Figure 10A). We transplanted $10^5$ $Ph^+$ B-ALL cells into pre-treated mice and collected animals collected pre-terminally at 15 days. Strikingly, bisphosphonate treatment resulted in a similar three-fold decrease in meningeal burden (Figure 10B, C), indicating that osteoclast activity, not RANKL, promoted B-ALL cell colonization and expansion in the meninges. Bisphosphonate inhibition of osteoclasts was incomplete (~33% of PBS controls) and further reduction in osteoclasts may enhance the ability of bisphosphonate to prevent B-ALL meningeal dissemination.

B-ALL cells express osteoclast activators *RANKL* and *TNFα.*

Given the observed increase in osteoclasts abundance, it is likely that B-ALL cells stimulate osteoclast differentiation. As osteoclast differentiation is regulated by a well-defined list of proteins, we performed a candidate qPCR screen for osteoclast regulators upregulated in B-ALL cell lines. From the 16 genes we tested, we identified augmented *Rankl* and *Tnfα* expression in B-ALL cells (Figure 11A, $P < 0.0004$, $P < 0.0001$ respectively). *Rankl* is the essential factor for osteoclast differentiation.[128,129] *Tnfα* induces stromal expression of *Rankl*[130] and can drive osteoclastogenesis directly.[131,132] Alternatively, the other candidates were expressed at very low levels in B-ALL cells (*m-csf, Il-1α, Il-1β, Il-15, Opn, Mmp9, Mmp12,* and *Opg*) or were not expressed in either cell type (*Il-6, Il-34, sFrp-2, Dkk1, Mmp7, Pthrp,* and *Pth*). Thus, B-ALL cells promote osteolysis by driving osteoclast differentiation by RANKL and/or TNFα.

CRISPR/Cas9 exposed single cell clones fail to give rise to leukemia *in vivo*

With the recent advent and accessibility of the CRISPR/Cas9 technology to sequence specifically target and mediate gene editing in cells,[133,134] we investigated the necessity of tumor-secreted

RANKL by editing the genomic locus of *Rankl* to disrupt and remove expression. We used the CRISPR/Cas9 technology to specifically target and remove the first exon of *Rankl* (Figure 12A). We electroporated complexed sgRNA/Cas9 into $Ph^+$ B-ALL cells for short term editing without sustained expression of Cas9. Electoporation successfully mediated uptake of the RNA/protein complex with minimal cell death, and resulted in deletion of the first exon (Figure 12B). Genotyping of single cell clones was confirmed by sequencing of the junctions (data not shown) and by qPCR validation of *Rankl* levels (Figure 12C). Furthermore, the editing was specific for *Rankl*, as expression of *Tnfα* was not affected by *Rankl* deletion (Figure 12D).

Unfortunately, *in vivo* transplantation of the $Ph^+$ *Rankl*$^{+/+}$ or $Ph^+$ *Rankl*$^{-/-}$ B-ALL cells failed to give rise to leukemia in both non-irradiated and irradiated recipient mice, suggesting that the Cas9 editing process or single cell cloning process affected the tumorigenicity of these cells. Collaborators have observed similar loss of tumorigenicity after Cas9 mediated editing and suggested a loss of *BCR-ABL* expression, but single cell clones maintained *BCR-ABL* expression, albeit at lower levels than $Ph^+$ B-ALL cells never exposed to Cas9 (data not shown).

Tumor secreted RANKL promotes meningeal dissemination

We assessed the necessity of tumor-derived RANKL by knockdown of *Rankl* expression in $Ph^+$ B-ALL cells using a pLKO.1 shRNA lentiviral vector. shRANKL #4 efficiently knocked down 80% of *Rankl* mRNA, (Figure 13A), but did not decrease the rate of proliferation in the B-ALL cells *in vitro* (Figure 13B). Thus, tumor-derived RANKL likely indirectly supports B-ALL cell growth through effects on the bone microenvironment, rather than acting autocrinely to drive B-ALL cell proliferation. To test the necessity of tumor-derived RANKL, we transplanted $10^5$ shRANKL or shSCRAMBLE $Ph^+$ B-ALL cells into irradiated, 4-week-old syngeneic C57BL/6 recipients. Strikingly, shRANKL $Ph^+$ B-ALL cells were slower to infiltrate the diploë and meninges at the pre-terminal time point (11 days post-transplantation) and reduced the ability of $Ph^+$ B-ALL cells to induce osteolysis throughout the course of tumorigenesis (Figure 13C). Thus, although reduced *Rankl* is not sufficient to eliminate meningeal dissemination, tumor-derived RANKL plays a role in $Ph^+$ B-ALL driven osteolysis, which likely supports early colonization and establishment of B-ALL cells in the diploe and meninges.

Inability to knockdown of *Tnfα* by shRNA

Given the effects of the CRISPR/Cas9 editing and single cell cloning process had on the tumorigenicity of the $Ph^+$ B-ALL cells, we used shRNA technology to knockdown expression of *Tnfα*. Unfortunately, using 11 different shRNA targeting sequences in two separate vector systems (pLKO.1 and miR-E[110]), we were unable to successfully decrease *Tnfα* mRNA by an appreciable amount (Figure 14). Although we cannot explain this inability to knockdown *Tnfα*, it is possible that the $Ph^+$ B-ALL cells are dependent upon TNFα in an autocrine manner and any cells with appreciable knockdown are selected against. To get around this, we will use CRISPR/Cas9 to delete *Tnfα* for *in vitro* studies and test the efficacy of inhibiting TNFα signaling *in vivo* by other methods.

*Rankl* and *Tnfα* expression is driven by *BCR-ABL*

Our data suggests that tumor-derived RANKL (and TNFα) likely drive osteoclast activity *in vivo* to support meningeal dissemination. As the tumorigenicity of the $Ph^+$ B-ALL model is dually driven by overexpression of *BCR-ABL* and loss of *Arf*, we investigated whether one or both of

these genetic lesions drove *Rankl* and *Tnfα* expression. We measured *Rankl* and *Tnfα* expression levels in wildtype B-cells or $Arf^{-/-}$ B-cells overexpressing *BCR-ABL* (Figure 15A). Impressively, *BCR-ABL* was sufficient to double *Rankl* expression ($P = 0.0109$), which was further increased with $Arf^{-/-}$ loss ($P < 0.0001$), and increase *Tnfα* expression five-fold ($P < 0.0001$) (Figure 15B). BCR-ABL reproducibly induced *Rankl* and *Tnfα,* with the greatest expression observed in B-cells with a lower infection efficiency (30-50%) (Figure 15C). Induction of *Rankl* and *Tnfα* occurred within 48 hours after infection with *BCR-ABL*, suggesting that the signaling downstream of BCR-ABL is likely direct (Figure 15D). *BCR-ABL* also induced *Rankl* and *Tnfα* expression in *Eμ-Myc* cell lines, although the level of *Rankl* and *Tnfα* induction varied between different cell lines (Figure 15E). The variability was likely due to different genetic alterations acquired over the course of the tumorigenesis process that gave rise to the *Eμ-Myc* cell lines. Thus, *BCR-ABL* overexpression induces *Rankl* and *Tnfα* expression in two different B-cell culture systems, strongly indicating that BCR-ABL likely directly drives *Rankl* and *Tnfα* expression in $Ph^+$ B-ALL cells.

*Rankl* expression is mediated by *Stat5a*

The aberrantly constitutively active kinase activity of BCR-ABL likely drives expression of *Rankl* and *Tnfα* through phosphorylation of a transcription factor. As BCR-ABL phosphorylates and activates STAT proteins, we knocked down expression of the STAT proteins known to be involved in BCR-ABL signaling and/or constitutively activated in leukemias: *Stat1*, *Stat3*, *Stat5a*, and *Stat5b*.[68,135–137] Knockdown of *Stat1*, *Stat3*, and *Stat5b* in $Ph^+$ B-ALL cells did not decrease mRNA levels of *Rankl* and *Tnfα* (Figure 16A, B, C). However, moderate knock down of *Stat5a* decreased *Rankl* (Figure 16D, E). Although the decrease in *Rankl* mRNA was not statistically significant, *Stat5a* mRNA levels were only reduced by 40% and a greater knockdown is likely required to see a stronger effect on *Rankl* levels. Thus, BCR-ABL likely drives *Rankl* expression through aberrantly activated Stat5a.

Conclusions

Leptomeningeal dissemination (LMD) in human patients is frequently seen in patients with both precursor B-cell acute lymphoblastic lymphoma (B-ALL) and Burkitt Lymphoma (BL) and in fact, is so common that both groups of patients are treated prophylactically with intrathecal chemotherapy.[18,51,138] In a mouse model of each disease, we have demonstrated a high frequency for meningeal dissemination, which is associated with extensive osteolysis (Figures 6, 8). Furthermore, while early signs of the osteolysis can be seen at a time point during the middle of the course of $Ph^+$ B-ALL development, the bone degradation increases with tumor progression and is most extreme in the terminally ill mice (Figure 6B, C). It is possible that this relationship is correlative; we have shown that inhibition of osteoclast activity impairs the ability of $Ph^+$ B-ALL cells to colonize and expand within the meninges (Figure 9, 10). Although our study lacks a direct connect to the human clinical observations, we believe it may be unlikely that such a relationship would be observed in human patients due to an unawareness of the potential importance of osteolysis and meningeal dissemination in B-ALL. While advances in treatment have reduced the rate of meningeal dissemination through prophylactic intrathecal chemotherapy, fewer patients could be treated and spared the neurological side effects if better patient stratification separated out patients truly at risk for meningeal dissemination at relapse. When osteolysis is reported in human B-ALL patients, it is generally associated with joint or bone pain,[139,140] which may lead to infrequent examination for osteolysis in the skull. However,

given our demonstration of the strong relationship between osteolysis and meningeal dissemination in the $Ph^+$ B-ALL mouse mode, it may be underestimated in human patients rather than infrequent.

Although the mechanism of meningeal dissemination in leukemia, specifically B-ALL, is currently being defined, studies have shown that the majority of human B-ALL cells are able to traffic to the meningeal layers the a xenograft model.[32] Others have reported factors that support B-ALL growth in low serum conditions or prevent apoptosis induced by chemotherapies and suggested that these proteins may support *in vivo* CSF survival and resistance to chemotherapy, but fail to provide any *in vivo* evidence to support these claims.[34,35] Unlike the previous studies, our data demonstrates that the ability of $Ph^+$ B-ALL cells to manipulate osteoclasts *in vivo* dramatically supports their ability to colonize and expand within the meninges (Figures 9, 10, 13). We have shown that the osteoclast activity is important for meningeal infiltration, which is most relevant to human patients in the context of preventing meningeal dissemination at relapse. Although the transplantation experiments described here do not represent a relapse state of disease, we have begun to model relapse by pretreating mice with bisphosphonate (to mimic prophylactic treatment following initial chemotherapy induced remission) and transplanting 200 $Ph^+$ B-ALL cells into each mouse (to mimic low level residual disease). The preliminary results in a small cohort of mice suggest that bisphosphonate treatment increase disease free survival as none of the mice have died at 7 weeks post-transplantation of the $Ph^+$ B-ALL cells, but half of the PBS treated mice have (N=6 for each group) (data not shown). Thus, targeting the relationship between $Ph^+$ B-ALL cells and osteoclasts may provide clinical benefit for preventing relapse in the CNS.

The majority of the information about the signaling events downstream of *BCR-ABL* is based on studies of chronic myelogenous leukemia (CML), as it is core-driving lesion for all CML patients. We have clearly shown that *Rankl* and *Tnfα* expression are induced downstream of BCR-ABL signaling (Figure 15), an effect which is likely mediated through *Stat5a* signaling. Our observation that *Stat5a* functions as the down stream effector of BCR-ABL signaling is consistent with reports that *Stat5* is a downstream signaling molecule for *BCR-ABL*[68,141,142] and required for maintenance of *BCR-ABL* driven lymphoid leukemia.[143] Furthermore, a recent report has demonstrated, in a completely separate cell context, that *Stat5* was required for *Rankl* induction, in agreement with our results. Greater inhibition of *Stat5a* signaling will provide more definitive proof that *BCR-ABL* increases expression of *Rankl*, and potentially *Tnfα*, through *Stat5a* and we are conducting further experiments with alternate methods of repressing *Stat5a* activity.

In summary, our results have shown that successful modeling of meningeal dissemination in the $Ph^+$ B-ALL mouse model revealed a surprising relationship between meningeal dissemination and osteoclast activity. The B-ALL tumor cells were able to induce the osteoclast activity through *Rankl* signaling, downstream of *BCR-ABL* signaling, to enrich their local environment and support their colonization and expansion within the meninges. Our findings suggest that osteolysis in human B-ALL patients, in particular $Ph^+$ B-ALL patients, should be assessed with careful attention to the skull and spine as sources of support for minimal residual disease.

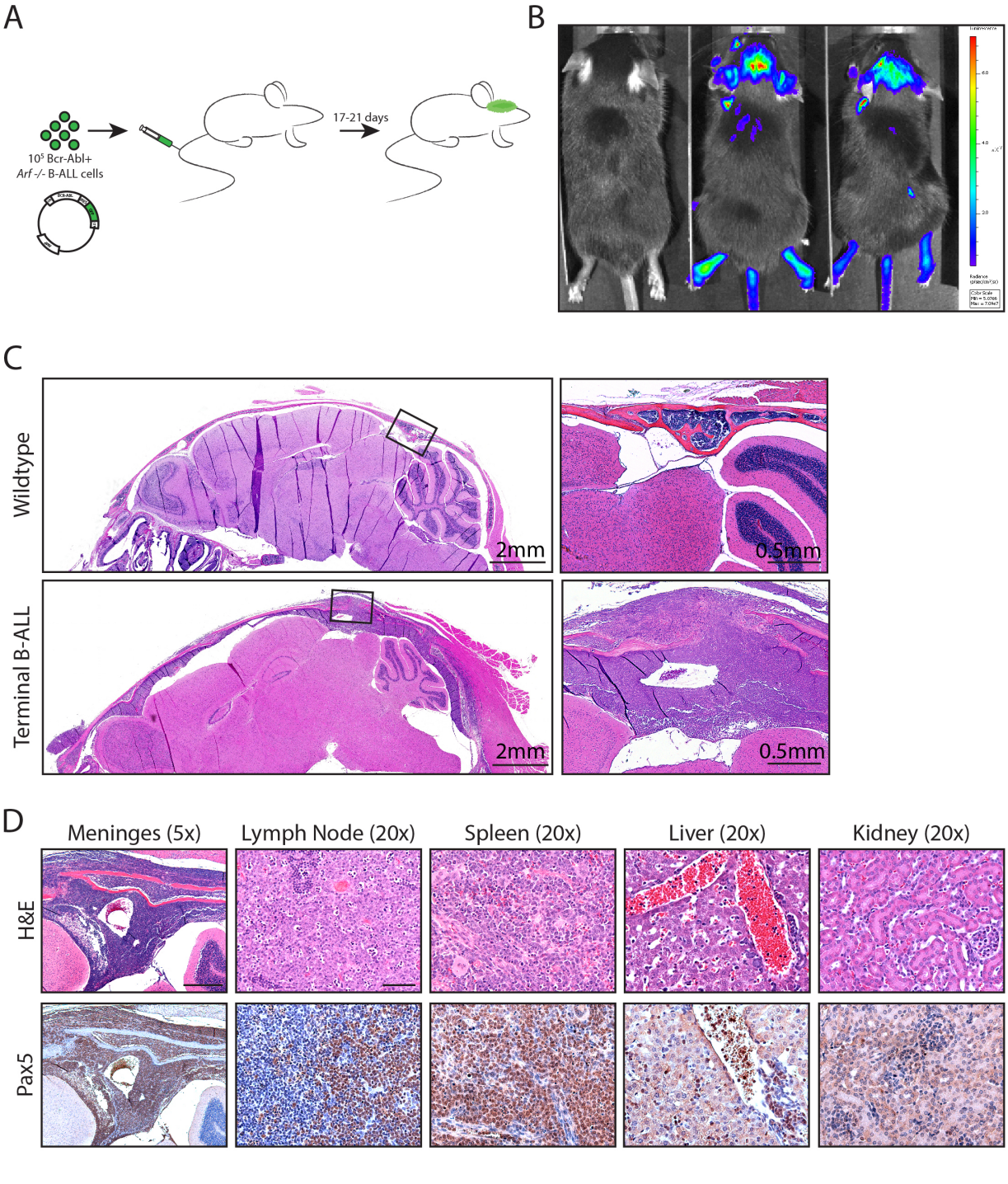
A
B
C
D
10⁵ Bcr-Abl+
Arf -/- B-ALL cells
17-21 days
Wildtype
Terminal B-ALL
2mm
0.5mm
2mm
0.5mm
Meninges (5x)
Lymph Node (20x)
Spleen (20x)
Liver (20x)
Kidney (20x)
H&E
Pax5

**Figure 4. Ph$^+$ *Arf*$^{-/-}$ induced B-ALL displays extensive meningeal dissemination. A.** Ph$^+$ B-ALL was modeled in mice though *BCR-ABL* overexpression in *Arf*$^{-/-}$ B-cells. $10^5$ GFP or luciferase labeled Ph$^+$ *Arf*$^{-/-}$ B-ALL cells were intravenously transplanted into 4-6 week old syngeneic mice and collected at the terminal stage (17-20 days). **B.** *In vivo* bioluminescent imaging revealed B-ALL tumor burden location. Compared to tumor-free mice (left), B-ALL mice (middle, right) displayed a high density of luciferase+ B-ALL cells in the head with minimal signal in other organs such as the lymph nodes or spleen. **C.** H&E staining revealed that meningeal infiltration was extensive in terminal B-ALL (right) mice, compared to tumor free (left) mice. Inset images show the lambdoid suture. B-ALL dissemination to the meningeal layers resulted in substantial expansion of the meningeal layers and suture tissue by disseminated B-ALL cells. **D.** B-ALL cells disseminated to a variety of different organs. H&E staining and Pax5 staining (for B-cells) of the meninges, hematopoietic (lymph node and spleen), and non-hematopoietic (liver and kidney) organs in terminal B-ALL mice revealed B-ALL cells dissemination to all organs, except the kidney, with preferential and extensive dissemination in the cranial meninges. 5x scale bars = 5 μm, 20x scale bars = 50 μm.

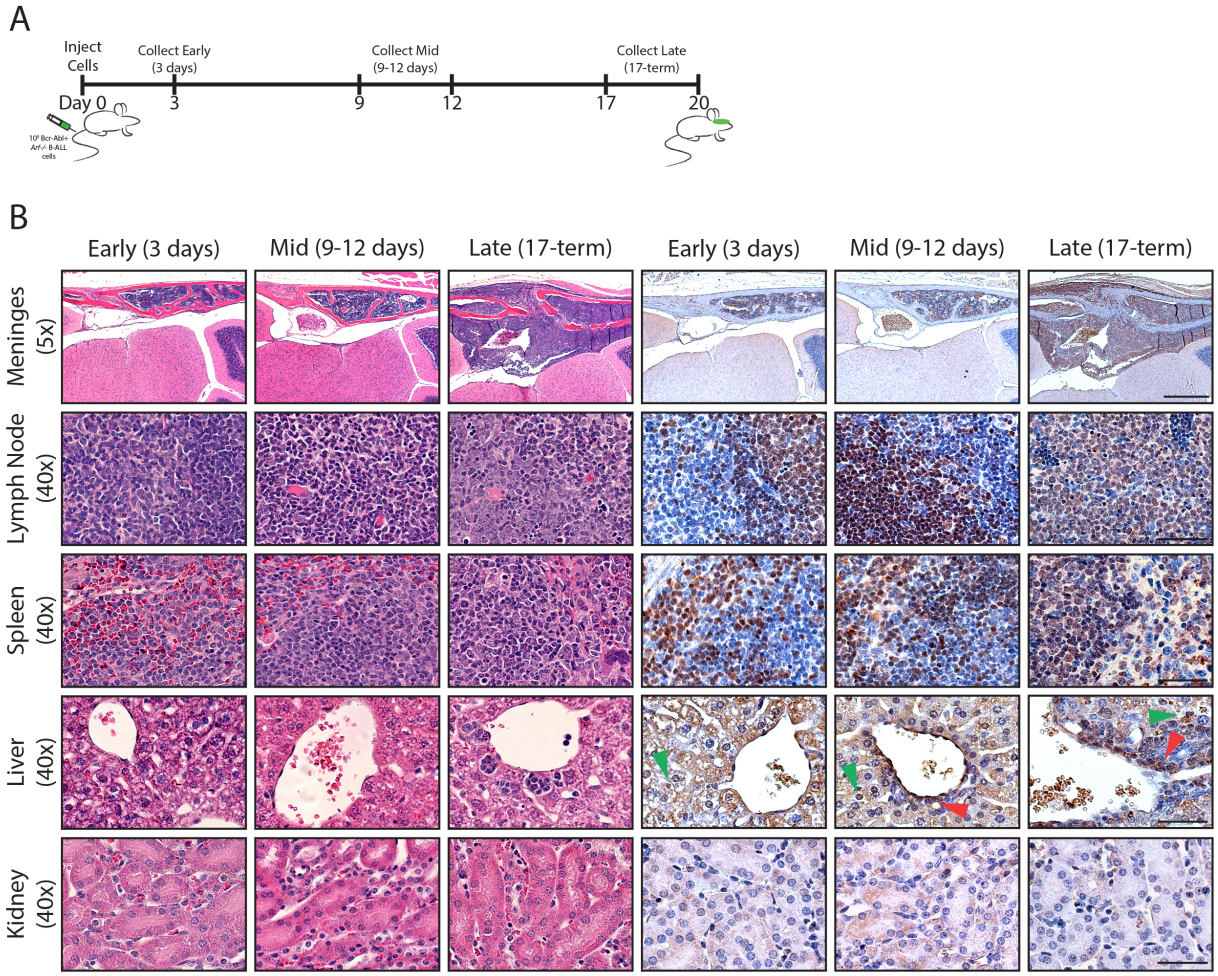


**Figure 5. Dissemination kinetics reveal preferential B-ALL expansion in the meninges. A.** Dissemination kinetics were examined by analysis of tumor dissemination over time. B-ALL mice ere collected every 2-3 days after transplantation to track the kinetics of dissemination to different tissues. **B.** Although organ seeding by B-ALL cells as comparable early in dissemination, B-ALL cells preferentially expanded in the meningeal layers. B-ALL cells were identified in all organs except the kidney and displayed similar dissemination kinetics at the early (3 days) and middle (9-12 days) time point by H&E staining and Pax5 immunohistochemistry of meninges, hematopoietic and non-hematopoietic organs. At the late (17-20 days) time point, extensive expansion and tissue disruption was only observed in the meninges, with other organs maintaining some normal tissue architecture. In the liver, B-ALL cells ere either adjacent to blood vessels (red arrowheads) or amid hepatocytes (green arrowheads). 5x scale bars = 0.50 mm, 20x scale bars = 50 μm.

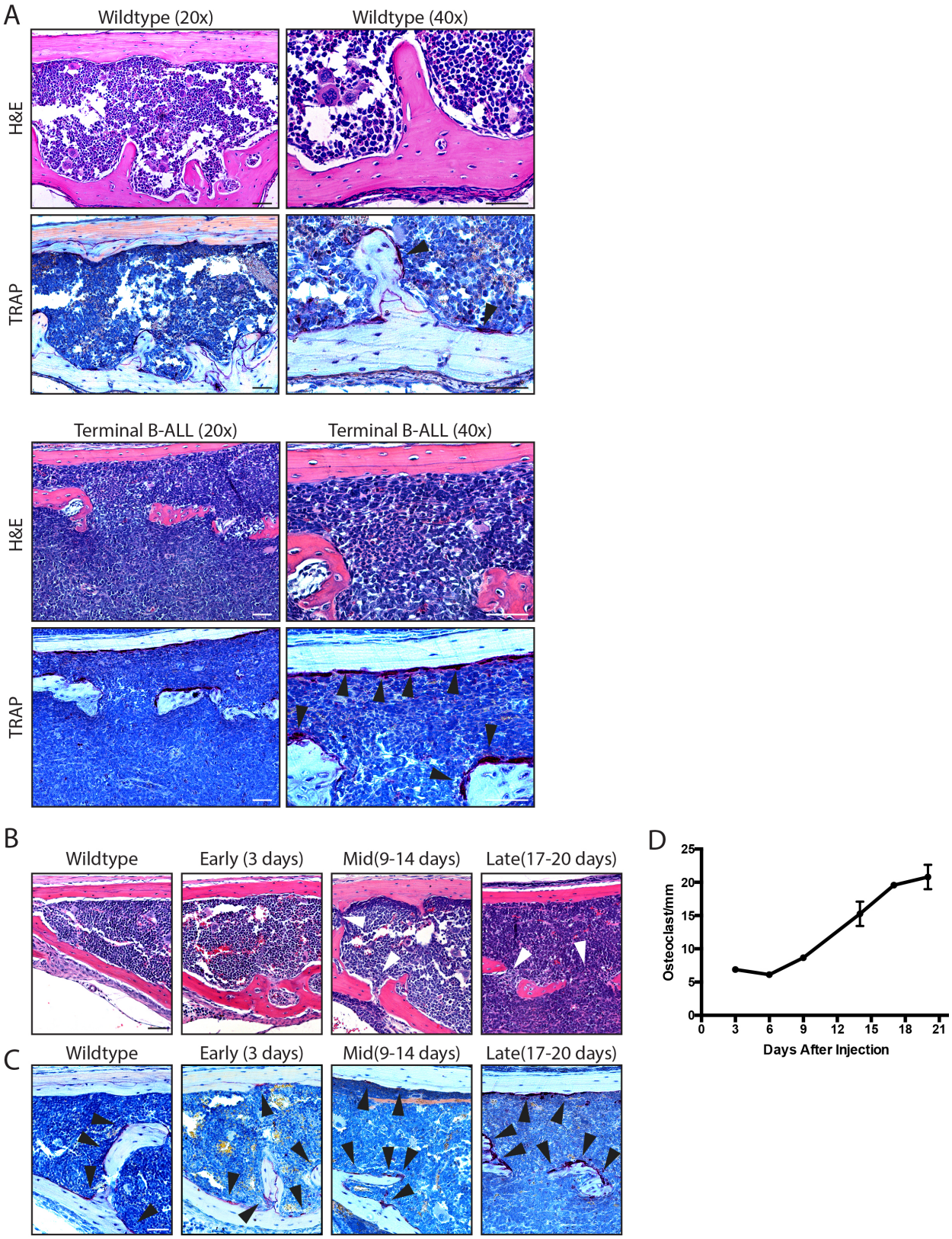
A
Wildtype (20x)
Wildtype (40x)
H&E
TRAP
Terminal B-ALL (20x)
Terminal B-ALL (40x)
H&E
TRAP
B
Wildtype
Early (3 days)
Mid(9-14 days)
Late(17-20 days)
C
Wildtype
Early (3 days)
Mid(9-14 days)
Late(17-20 days)
D
Osteoclast/mm
25
20
15
10
5
0
0
3
6
9
12
15
18
21
Days After Injection

**Figure 6. Meningeal dissemination is associated with osteoclast-mediated bone degradation.** **A.** Terminal B-ALL mice displayed osteolysis. H&E and Tartrate Resistant Acid Phosphatase (TRAP) staining revealed osteolysis in terminal B-ALL mice (right) compared to tumor-free mice (left). Diploë and calvarial bones in terminal B-ALL mice ere characterized by bone thinning and pitting (white arrows), loss of bone continuity, and an increased presence of osteoclasts (black arrowheads). Scale bars = 50 μm. **B-D.** Osteolysis and osteoclast number increased with tumor progression. H&E (B) and TRAP (C) staining of calvarial diploë and meninges over the course of B-ALL dissemination demonstrated an increase in both osteolysis and osteoclast number as tumors progressed. Scale bars = 50 μm. Quantification (D) confirmed that osteoclast number per mm of bone surface increased over the course of B-ALL dissemination. N = 3 mice for each time point, each point represents mean ± standard deviation.

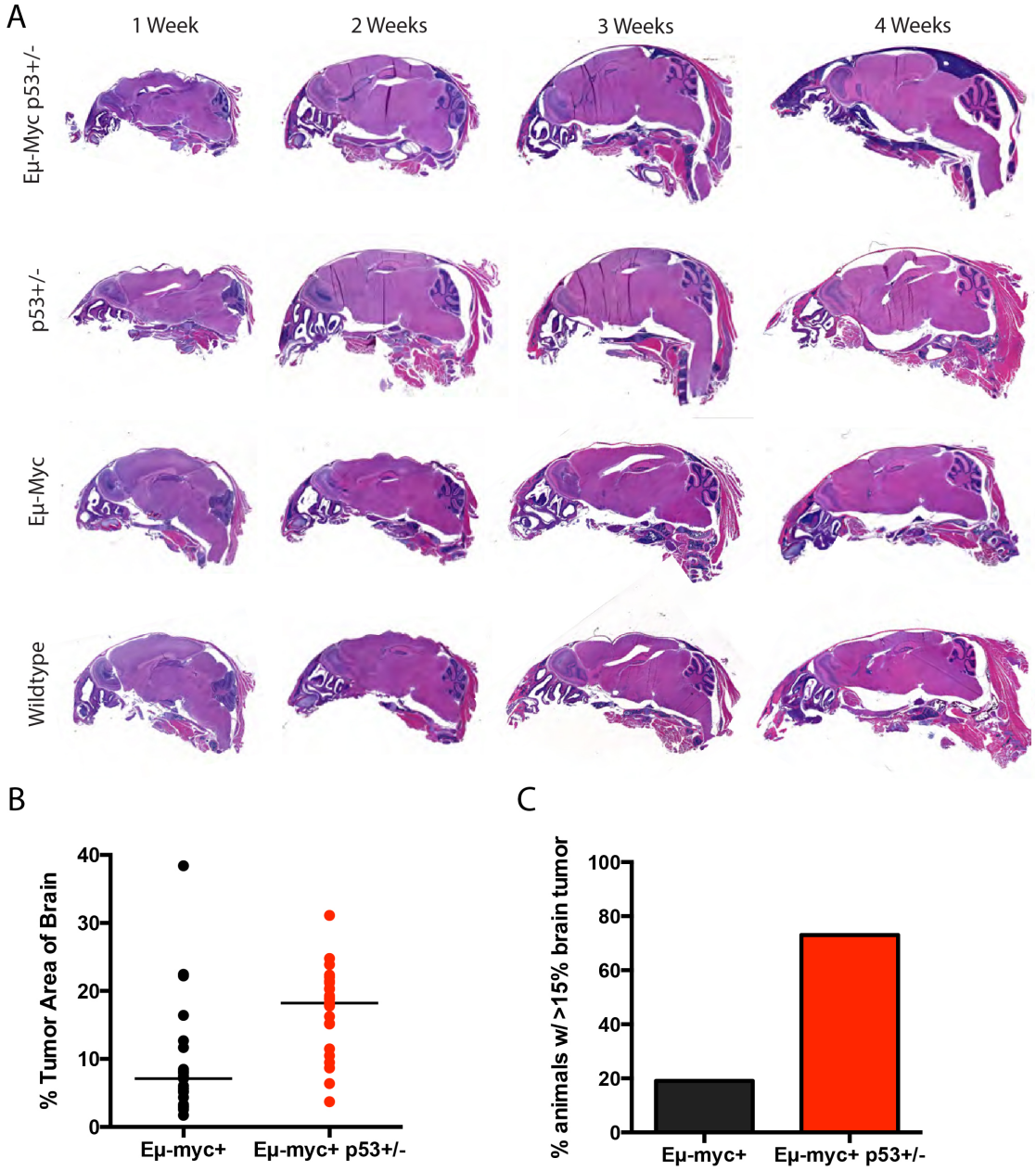


**Figure 7. Meningeal dissemination is seen in second hematopoietic mouse model. A.** Meningeal dissemination was observed in the Eμ-Myc mouse model of Burkitt Lymphoma. Spontaneous tumorigenesis was accelerated by loss of one allele of *p53*, with meningeal dissemination seen in *Eμ-Myc p53*$^{+/-}$ as early as 2 weeks after birth. **B.** Meningeal tumor burden was greater in *Eμ-Myc p53*$^{+/-}$ mice. Quantification of tumor burden in terminally ill *Eμ-Myc p53*$^{+/+}$ and *Eμ-Myc p53*$^{+/-}$mice, $P = 0.0013$. **C.** The frequency of substantial meningeal dissemination was greater in *Eμ-Myc p53*$^{+/-}$ mice. Quantification of the number of terminally ill *Eμ-Myc p53*$^{+/+}$ and *Eμ-Myc p53*$^{+/-}$mice with meningeal dissemination of greater than 15% of their skull area. $N \geq 9$.

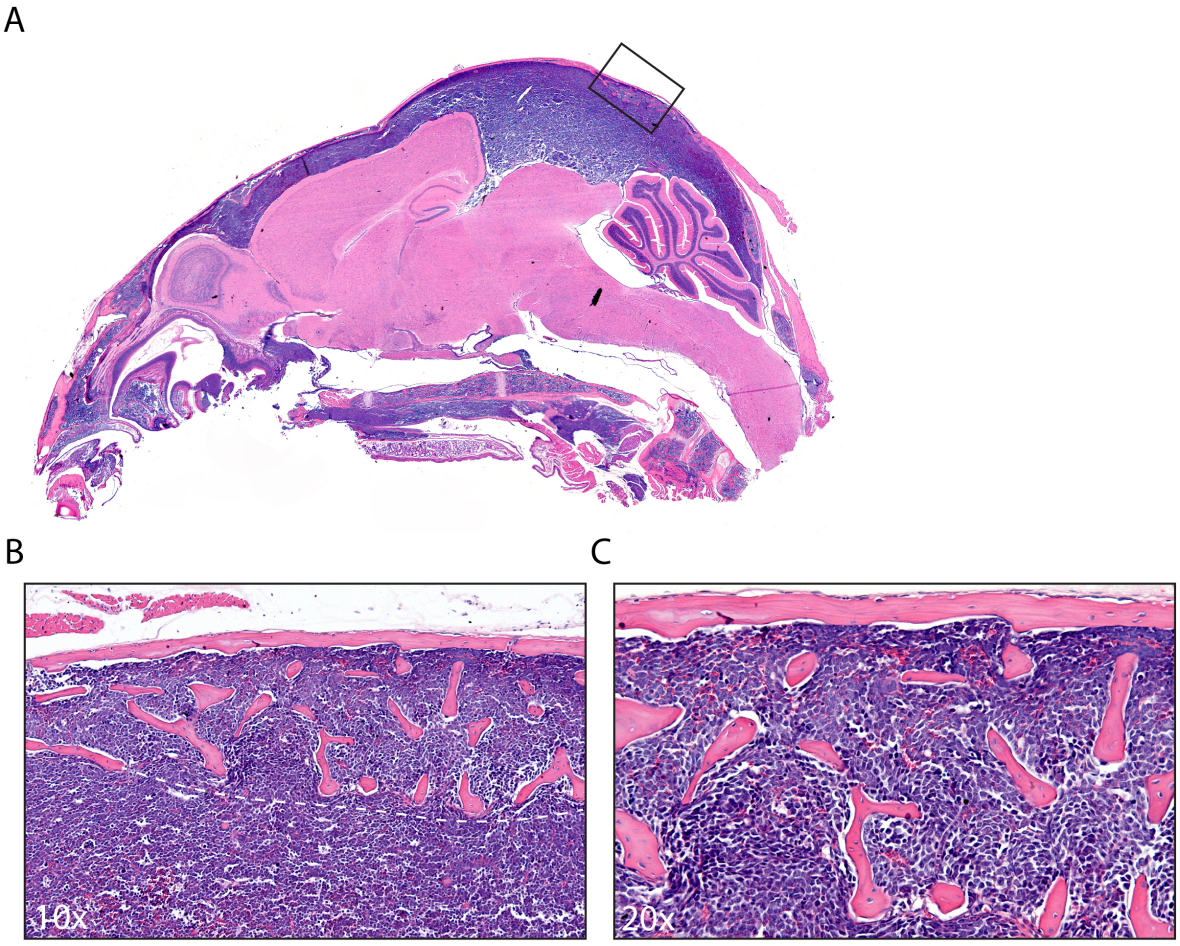


**Figure 8. Meningeal dissemination is associated with osteoclast-mediated osteolysis in the Eμ-Myc mouse model. A.** H&E staining of terminally ill *Eμ-Myc p53*$^{+/-}$ mice displayed extensive meningeal dissemination all along the top of the skull. **B, C.** Meningeal dissemination in *Eμ-Myc p53*$^{+/-}$ was associated with extensive osteolysis. H&E staining at higher magnification of the diploë at the lambdoid suture revealed bone thinning and pitting and loss of bone continuity. Dotted white line indicates where continuous bone should be.

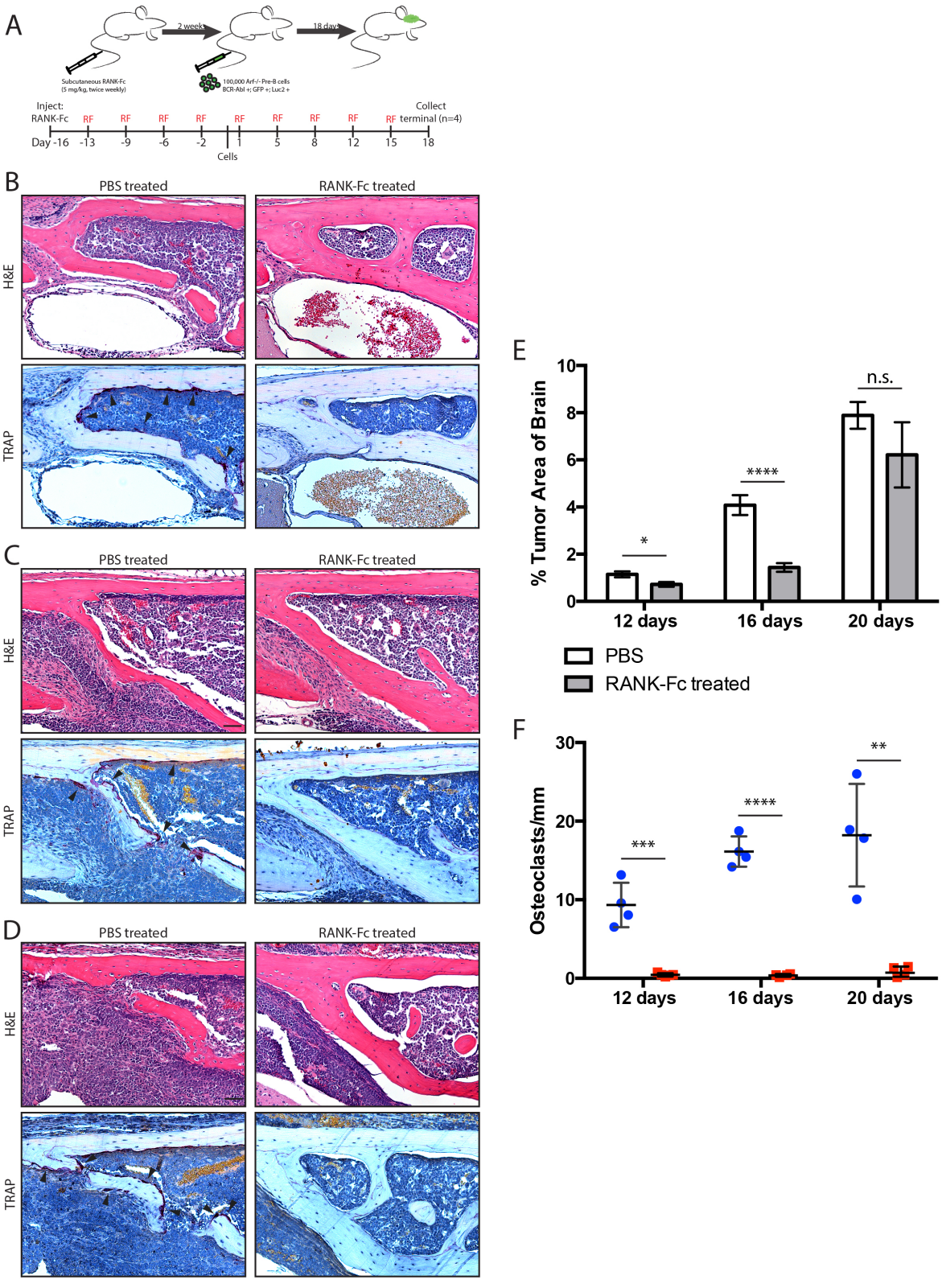
A
2 weeks
18 days
Subcutaneous RANK-Fc
(5 mg/kg, twice weekly)
100,000 Arf-/- Pre-B cells
BCR-Abl +; GFP +; Luc2 +
Inject:
RANK-Fc
Collect
terminal (n=4)
RF
Day -16
-13
-9
-6
-2
Cells
1
5
8
12
15
18
B
PBS treated
RANK-Fc treated
H&E
TRAP
C
PBS treated
RANK-Fc treated
H&E
TRAP
D
PBS treated
RANK-Fc treated
H&E
TRAP
E
% Tumor Area of Brain
10
8
6
4
2
0
*
****
n.s.
12 days
16 days
20 days
PBS
RANK-Fc treated
F
Osteoclasts/mm
30
20
10
0
***
****
**
12 days
16 days
20 days

**Figure 9. Osteoclast activity is necessary for early meningeal dissemination of B-ALL cells.** **A.** The necessity of osteoclast activity was assayed *in vivo* by RANK-Fc mediated inhibition of osteoclast differentiation. Mice ere pretreated with 10 mg/kg RANK-Fc or vehicle (PBS) subcutaneously for two weeks before transplantation of $Ph^+$ B-ALL cells and throughout experiment duration. Mice were collected at 12, 16, and 20 days post-transplantation. **B, C, D.** RANK-Fc treatment decreases osteoclast activity and early meningeal dissemination. H&E and TRAP staining of PBS (left) and RANK-Fc (right) treated mice at the 12 (B), 16 (C), and 20 (D) days post transplantation revealed a delay in B-ALL expansion in the meningeal layers and decreased meningeal tumor burden at 12 and 16 days post-transplantation, as evidenced by the decrease of deep purple B-ALL cells in the suture and meninges. Scale bar = 50 μm. **E.** Osteoclast inhibition delayed B-ALL cell expansion in the meninges. Quantification of meningeal dissemination in PBS (white bars) and RANK-Fc (grey bars) treated mice at the three different time points demonstrates a 3-fold decrease in tumor burden in treated mice. N > 4, average ± standard error of mean shown, * $P = 0.0147$, **** $P < 0.0001$. **F.** RANK-Fc effectively inhibited osteoclast differentiation. Quantification of osteoclast number per mm of bone surface in PBS (red) and RANK-Fc (blue) treated mice demonstrated complete inhibition of osteoclasts at all time points. N > 4, average ± standard deviation shown, ** $P = 0.0019$, *** $P = 0.0002$, **** $P < 0.0001$.

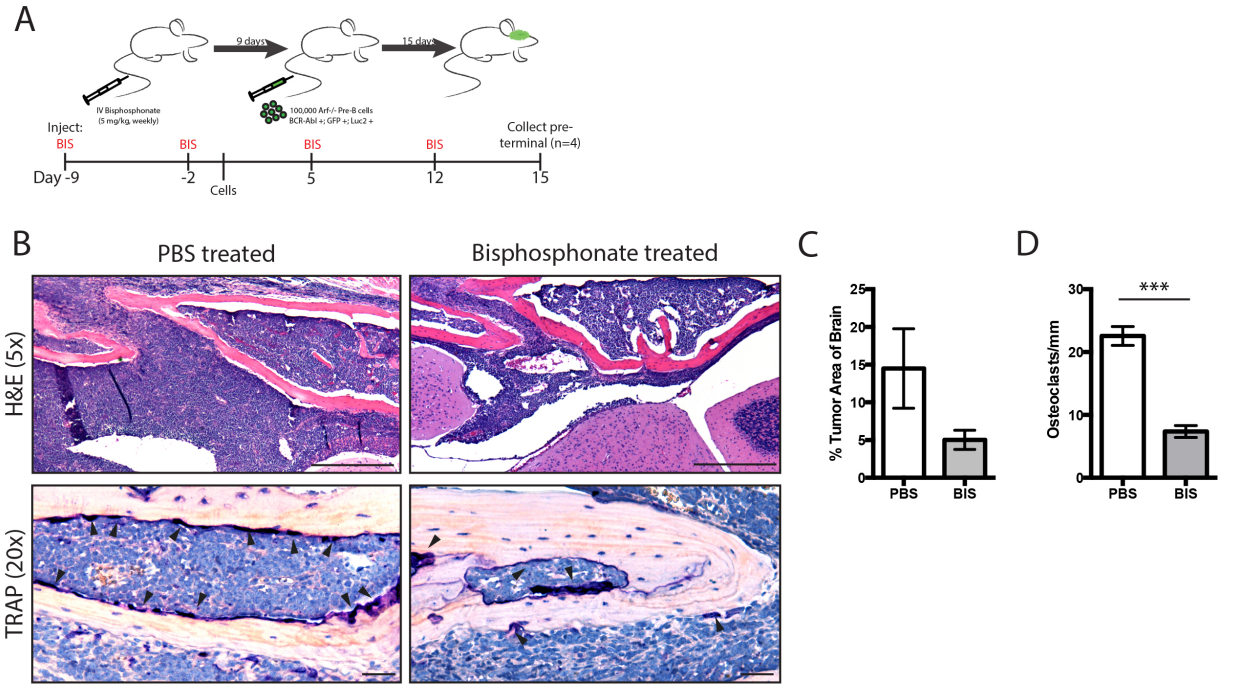


**Figure 10. Osteoclast activity, not just RANKL signaling, is required for meningeal dissemination of B-ALL cells. A.** The necessity of osteoclast activity, rather than RANKL, was assayed *in vivo* by bisphosphonate-mediated inhibition of osteoclast differentiation. Mice were pretreated weekly with 5 mg/kg bisphosphonate (pamidronate disodium pentahydrate) or vehicle (PBS) intravenously for two weeks before transplantation of of $Ph^{+}$ $Arf^{-/-}$ B-ALL cells and throughout experiment duration. Mice were collected pre-terminally at 15 days post-transplantation. **B.** Bisphosphonate treatment delayed B-ALL cell expansion and tumor burden in the meninges. H&E staining of PBS (left) and bisphosphonate (right) treated mice revealed that osteoclast activity promoted expansion of B-ALL cells in the meninges. TRAP staining of PBS and bisphosphonate treated mice indicated that osteoclast differentiation was incompletely blocked at the 5 mg/kg dosage of bisphosphonate. Scale bars = 50 µm. **C.** Osteoclast inhibition decreased B-ALL expansion in the meninges pre-terminally. Quantification of meningeal dissemination in PBS (white bars) and bisphosphonate (grey bars) treated mice revealed a 3-fold decrease in tumor burden in the meninges. N= 4, mean ± standard error of mean. **D.** Bisphosphonate treatment decreased the number of osteoclasts. Quantification of osteoclast number per mm of bone surface revealed an incomplete inhibition of osteoclast differentiation in bisphosphonate treated mice. N = 4, mean ± standard error of mean, *** $P = 0.0003$.

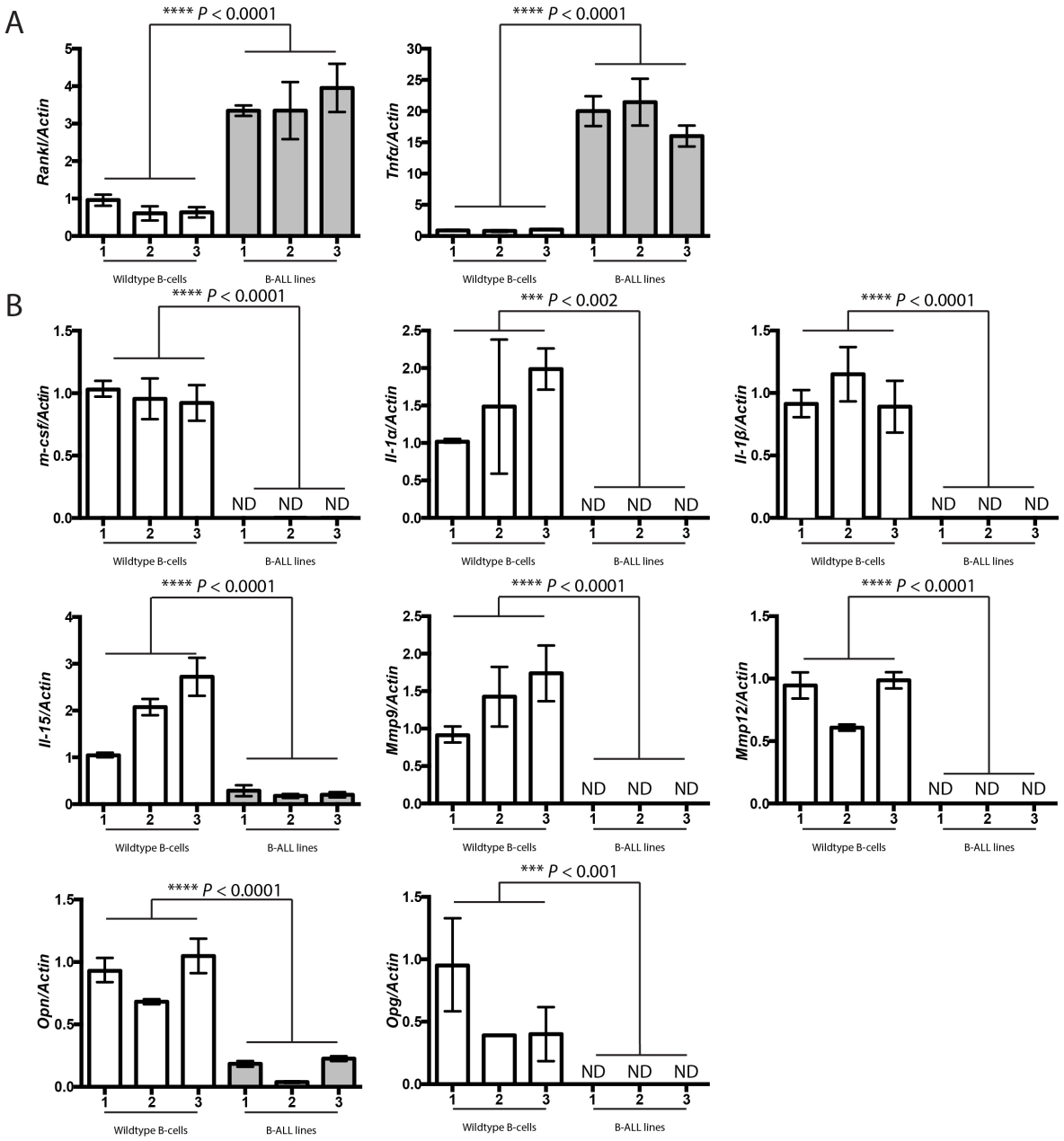


**Figure 11. qPCR screen reveals elevated levels of *Rankl* and *Tnfα* in B-ALL cells. A.** B-ALL cells express increased levels of *Rankl* and *Tnfα.* Relative expression levels of *Rankl* and *Tnfα* in 3 independent B-ALL cell lines (grey) are elevated compared to wildtype B-cells (white). Bars represent mean ± standard deviation**. ****** $P < 0.0001$. **B.** B-ALL cells express lower levels of other genes regulating osteoclast differentiation or expression patterns that would not promote osteoclast differentiation. Relative expression levels of *m-csf, Il-1α, Il-1β, Il-15, Mmp9, Mmp12, Opn,* and *Opg* in 3 independent B-ALL cell lines (grey) are elevated compared to wildtype B-cells (white). Bars represent mean ± standard deviation**.** ND = not detectable, bars represent mean ± standard deviation. *P* values as listed.

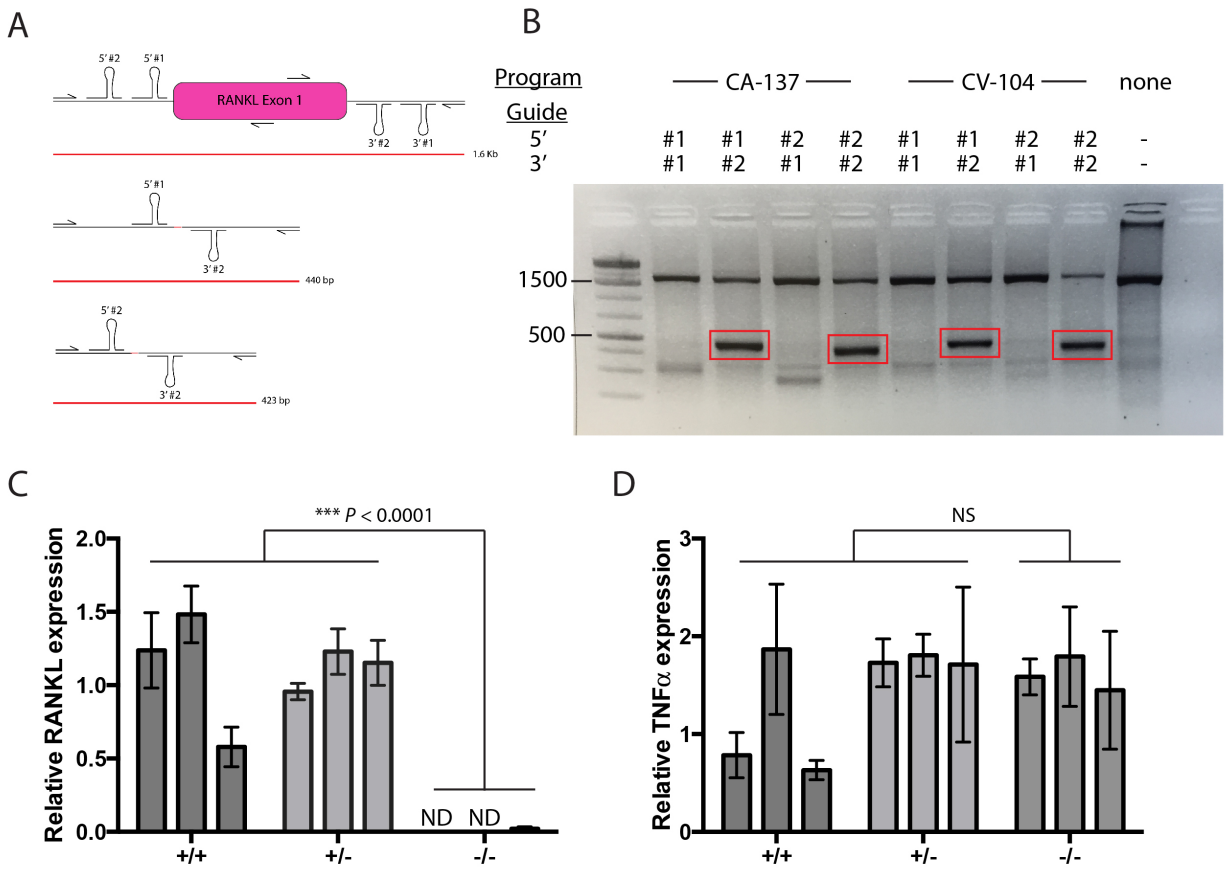


**Figure 12. CRISPR editing of *Rankl* specifically eliminates expression of *Rankl*. A.** To evaluate the necessity of tumor-secreted RANKL, B-ALL cells were edited with CRISPR to remove *Rankl.* Two pairs of sgRNAs and genotyping primers were designed for CRISPR/Cas9 mediated deletion of the first exon of *Rankl.* Unedited *Rankl* would produce a 1.6 kb band, while *Rankl* DNA edited with sgRNA 5' #1 and sgRNA 3' #2 or sgRNA 5' #2 and sgRNA 3' #2 would give bands of 440 bp or 423 bp, respectively. **B.** Electroporated complexed sgRNA/Cas9 protein edited the *Rankl* locus in B-ALL cells. Genotyping of electorporated B-ALL cells revealed B-ALL cell populations edited by sgRNA 5' #1 and sgRNA 3' #2 or sgRNA 5' #2 and sgRNA 3' #2 in both electroporation programs used. **C.** *Rankl* deletion resulted in elimination of *Rankl* mRNA levels. *Rankl* mRNAs were not detected or very lowly detected in *Rankl*$^{-/-}$ single cell clones, compared to *Rankl*$^{+/+}$ and *Rankl*$^{+/-}$ single cell clones. Bars represent mean ± standard deviation, **** $P < 0.0001$. **D.** *Rankl* deletion did not affect other mRNA levels. mRNA levels of *Tnfα* are unaffected in *Rankl*$^{+/+}$, *Rankl*$^{+/}$, and *Rankl*$^{-/-}$ single cell clones. Bars represent mean ± standard deviation.

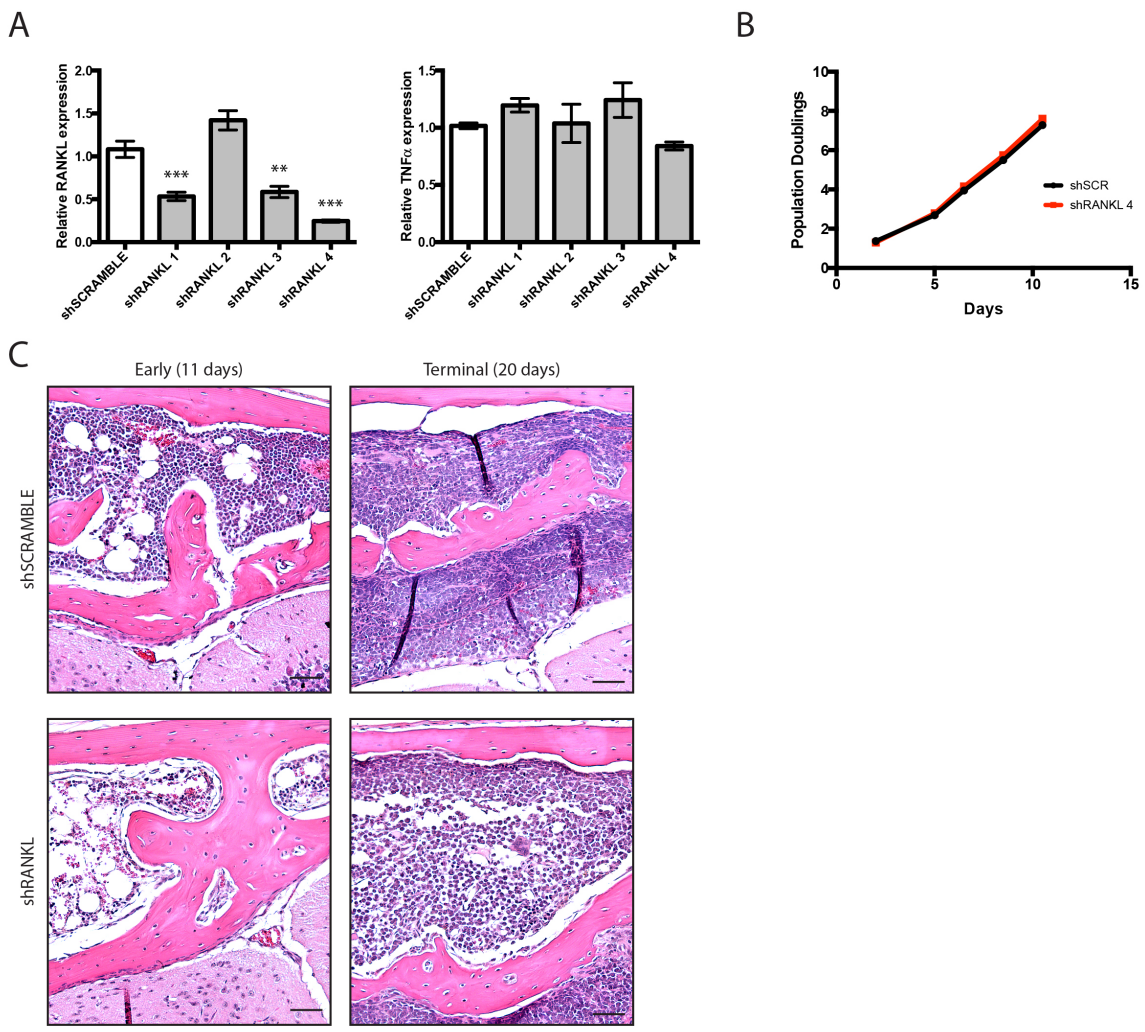


**Figure 13. shRNA knockdown of *Rankl* delays dissemination to the diploe and meninges. A.** mRNA levels of *Rankl*, but not *Tnfα*, are reduced by shRNA knockdown of with shRNAs #1, #3, and #4. Bars represent mean ± standard deviation, *** $P < 0.001$, **** $P < 0.0001$. **B.** *Rankl* knockdown does not affect proliferation. *In vitro* proliferation assay comparing growth kinetics of shRANKL #4 expressing B-ALL cells, compared to control shSCRAMBLE. **C.** B-ALL cells with reduced RANKL delays early meningeal dissemination. H&E staining of the diploe and meninges near the lambdoid suture of mice transplanted with shSCRAMBLE or shRANKL expressing B-ALL cells at an early (11 days post-transplantation) or terminal (20 days post transplantation) time point revealed tumor-secreted RANKL contributed to enhancing the meningeal microenvironment to promote meningeal dissemination of B-ALL cells, but did not prevent eventual infiltration of the meninges. N=4, scale bars = 50 μm.

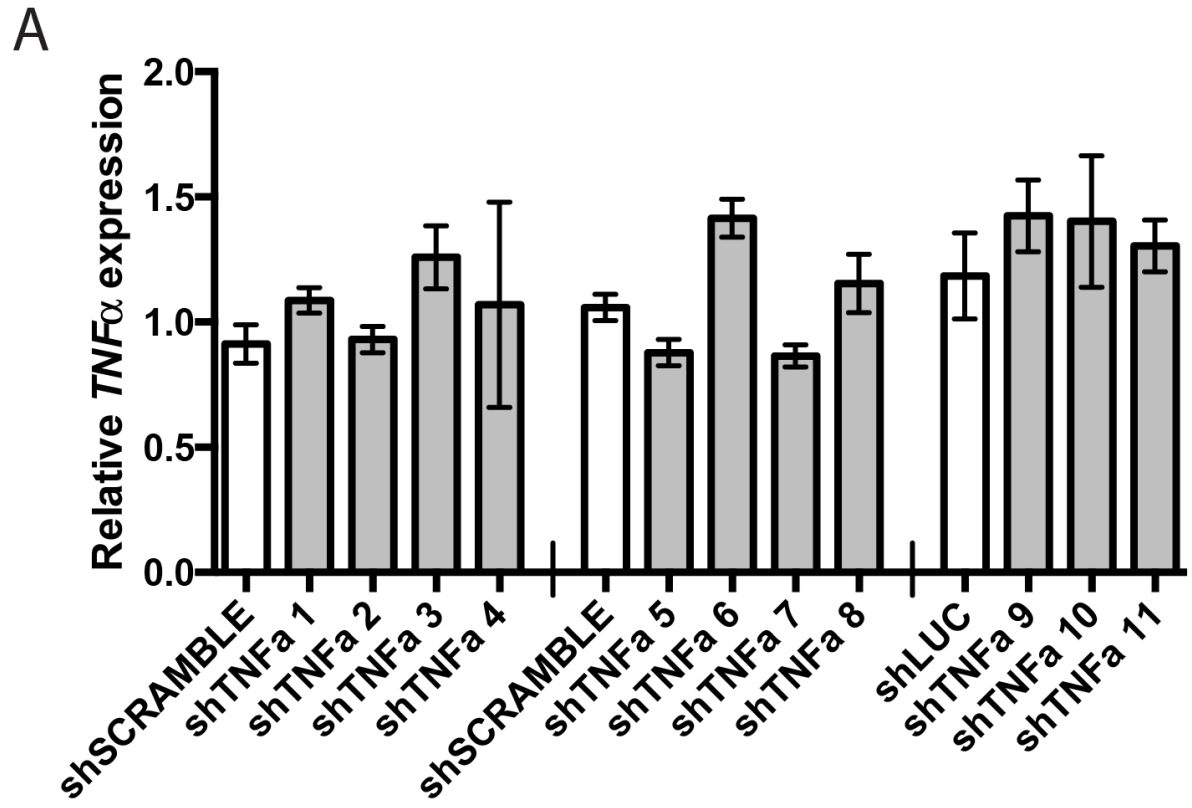


**Figure 14. Expression of 11 different *Tnfα* shRNAs fails to reduce mRNA levels of *Tnfα*. A.** mRNA levels of *Tnfα* were not reduced by 11 different shRNA targeting sequences in two different viral vector systems. Bars represent average ± standard deviation.

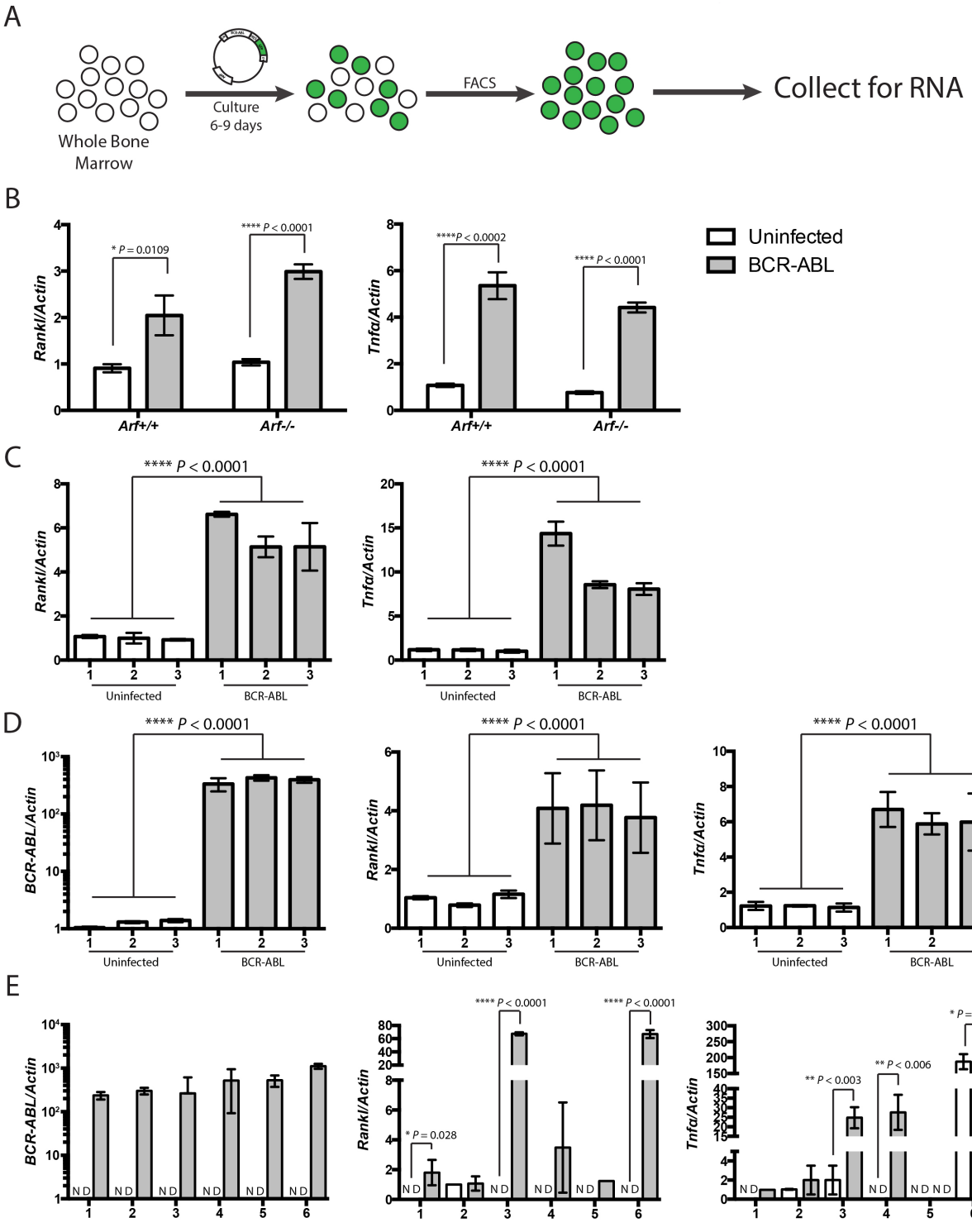
A
Whole Bone Marrow
Culture 6-9 days
FACS
Collect for RNA
B
Uninfected
BCR-ABL
Rankl/Actin
Tnfa/Actin
* P = 0.0109
**** P < 0.0001
****P < 0.0002
Arf+/+
Arf-/-
C
Uninfected
BCR-ABL
D
BCR-ABL/Actin
E
ND
* P = 0.028
** P < 0.003
** P < 0.006
* P = 0.027

**Figure 15. *BCR-ABL* overexpression drives increased *Rankl* and *Tnfα* expression in B-cells and Eμ-Myc lymphoma cells. A.** The ability of BCR-ABL to drive expression of *Rankl* and *Tnfα* was tested by overexpression of *BCR-ABL.* Briefly, freshly harvested bone marrow cells from 4-6 week old mice ere cultured in 2.5 ng/mL IL-7 and infected with MSCV-BCR-ABL-IRES-GFP, sorted for GFP positive cells, and collected for RNA. **B.** *BCR-ABL* was the dominant genetic lesion driving *Rankl* and *Tnfα* expression. mRNA levels of *Rankl* and *Tnfα* were increased by *BCR-ABL* overexpression (gray bars) in $Arf^{+/+}$ and $Arf^{-/-}$ B-cells, compared to uninfected (white bars) to determine if one or both of the critical genetic lesions in this model of $Ph^{+}$ B-ALL was responsible for the upregulation of *Rankl* and *Tnfα* mRNA. *BCR-ABL* overexpression was the predominant factor driving increased levels of both *Rankl* and *Tnfα.* Bars represent average ± standard deviation, *P* values as listed. **C.** Lower levels of *BCR-ABL* drive higher expression of *Rankl* and *Tnfα. BCR-ABL* was overexpressed in three independent wildtype B-cell cultures and drove increased mRNA levels of *Rankl* and *Tnfα.* Bars represent average ± standard deviation, **** $P < 0.0001$. **D.** *BCR-ABL* overexpression increased mRNA levels of *Rankl* and *Tnfα* at 48 hours post-infection. Levels of *BCR-ABL, Rankl,* and *Tnfα* were increased in wildtype B-cells in only 48 hours after infection, suggesting increased *Rankl* and *Tnfα* levels are driven directly by BCR-ABL, rather than downstream signaling pathways. Bars represent average ± standard deviation, **** $P < 0.0001$. **E.** BCR-ABL can increase Rankl and *Tnfα* mRNA levels in lymphoma cell lines. mRNA levels of *BCR-ABL*, *Rankl*, and *Tnfα* are increased in some *Eμ-Myc* and *Eμ-Myc* $p53^{+/-}$ lymphoma cell lines, suggesting genetic mutations accumulated in the lymphoma cell lines may be permissive or inhibitory on BCR-ABL mediated signaling. Bars represent average ± standard deviation, *P* values as listed.

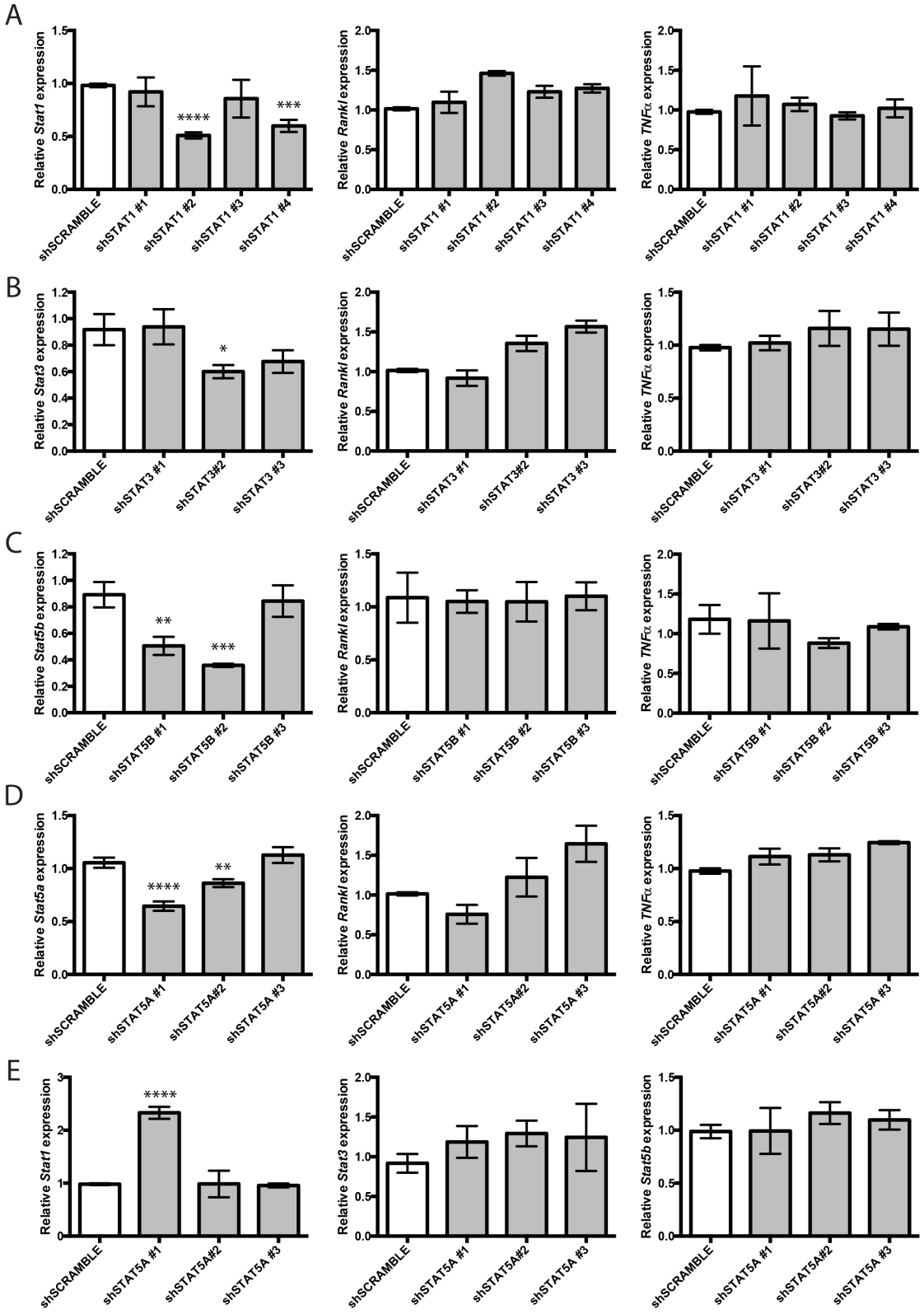
A
Relative Stat1 expression
****
***
Relative Rankl expression
Relative TNFα expression
shSCRAMBLE
shSTAT1 #1
shSTAT1 #2
shSTAT1 #3
shSTAT1 #4
B
Relative Stat3 expression
*
Relative Rankl expression
Relative TNFα expression
shSCRAMBLE
shSTAT3 #1
shSTAT3#2
shSTAT3 #3
C
Relative Stat5b expression
**
***
Relative Rankl expression
Relative TNFα expression
shSCRAMBLE
shSTAT5B #1
shSTAT5B #2
shSTAT5B #3
D
Relative Stat5a expression
****
**
Relative Rankl expression
Relative TNFα expression
shSCRAMBLE
shSTAT5A #1
shSTAT5A#2
shSTAT5A #3
E
Relative Stat1 expression
****
Relative Stat3 expression
Relative Stat5b expression
shSCRAMBLE
shSTAT5A #1
shSTAT5A#2
shSTAT5A #3

**Figure 16. *Stat5a* may mediate *BCR-ABL* induction of *Rankl*.** A, B. mRNA levels *Stat1* (A), *Stat3* (B), and *Stat5b* (C) are reduced by shRNA knockdown (gray bars) compared to control scramble shRNA (white bars), while knockdown did not affect either *Rankl* or *Tnfα* expression levels. Bars represent average ± standard deviation, * $P = 0.0216$, ** $P = 0.0048$, *** $P < 0.0007$, **** $P < 0.0001$. C. qPCR confirms *Stat5a* knockdown by shRNA and a corresponding slight reduction in *Rankl*, but not *Tnfα*. Bars represent average ± standard deviation, ** $P = 0.0055$, **** $P < 0.0001$. D. *Stat1*, *Stat3*, and *Stat5b* mRNA levels in B-ALL cells expressing shRNAs against *Stat5a*. Bars represent average ± standard deviation, **** $P < 0.0001$.

## References

1. Jemal, A., Siegel, R. & Miller, K. D. American Cancer Society - Cancer Facts & Statistics. (2016). at <https://cancerstatisticscenter.cancer.org/#/>
2. Langley, R. R. & Fidler, I. J. The seed and soil hypothesis revisited--the role of tumor-stroma interactions in metastasis to different organs. *Int. J. Cancer* **128,** 2527–35 (2011).
3. Paget, S. The Distribution of Secondary Growths in Cancer of the Breast. 1989. *Cancer Metastasis Rev.* **8,** 98–101 (1989).
4. Valastyan, S. & Weinberg, R. a. Tumor metastasis: Molecular insights and evolving paradigms. *Cell* **147,** 275–292 (2011).
5. Kang, Y. *et al.* A multigenic program mdeiating breast cancer metastasis to bone. *Cancer Cell* **3,** 537–549 (2003).
6. Corey, E. *et al.* Establishment and characterization of osseous prostate cancer models: intra-tibial injection of human prostate cancer cells. *Prostate* **52,** 20–33 (2002).
7. Weller, R. O. MICROSCOPIC MORPHOLOGY AND HISTOLOGY OF THE HUMAN MENINGES. *Morphologie* **89,** 22–34 (2005).
8. Aspelund, A. *et al.* A dural lymphatic vascular system that drains brain interstitial fluid and macromolecules. *J. Exp. Med.* **212,** 991–9 (2015).
9. Barshes, N., Demopoulos, A. & Engelhard, H. H. Anatomy and physiology of the leptomeninges and CSF space. *Cancer Treat. Res.* **125,** 1–16 (2005).
10. Adeeb, N. *et al.* The intracranial arachnoid mater. *Child's Nerv. Syst.* **29,** 17–33 (2013).
11. Adeeb, N. *et al.* The pia mater: a comprehensive review of literature. *Child's Nerv. Syst.* **29,** 1803–1810 (2013).
12. Nicolas, D. S. & Weller, R. O. The fine anatomy of the human spinal meninges: A light and scanning electron microscopy study. *J. Neurosurg.* **69,** 276–282 (1988).
13. Basu, S. K., Remick, S. C., Monga, M. & Gibson, L. F. Breaking and entering into the CNS: clues from solid tumor and nonmalignant models with relevance to hematopoietic malignancies. *Clin. Exp. Metastasis* **31,** 257–267 (2014).
14. Gril, B., Evans, L., Palmieri, D. & Steeg, P. S. Translational research in brain metastasis is identifying molecular pathways that may lead to the development of new therapeutic strategies. *Eur. J. Cancer* **46,** 1204–1210 (2010).
15. Whitsett, T. G. *et al.* Molecular determinants of lung cancer metastasis to the central nervous system. *Transl. Lung Cancer Res.* **2,** 273–283 (2013).
16. Chamberlain, M. C. Leptomeningeal metastasis. *Curr. Opin. Oncol.* **22,** 627–635 (2010).
17. Weil, R. J., Palmieri, D. C., Bronder, J. L., Stark, A. M. & Steeg, P. S. Breast Cancer Metastasis to the Central Nervous System. *Am. J. Pathol.* **167,** 913–920 (2005).
18. Abrey, L. E., Chamberlain, M. C. & Engelhard, H. H. *Leptomeningeal Metastasis*. *J. Chem. Inf. Model.* **53,** (2013).
19. Chamberlain, M. C. *et al.* Leukemic and lymphomatous meningitis: incidence, prognosis and treatment. *J. Neurooncol.* **75,** 71–83 (2005).
20. Kesari, S. & Batchelor, T. T. Leptomeningeal metastases. **21,** 25–66 (2003).
21. Martins, S. J. *et al.* Meningeal carcinomatosis in solid tumors. *Arq. Neuropsiquiatr.* **69,** 973–980 (2011).
22. Le Rhun, E., Taillibert, S. & Chamberlain, M. C. Carcinomatous meningitis: Leptomeningeal metastases in solid tumors. *Surg. Neurol. Int.* **4,** S265–88 (2013).
23. Surapaneni, U. R. *et al.* Central nervous system relapse in adults with acute lymphoblastic leukemia. *Cancer* **94,** 773–779 (2002).
24. Mareel, M., Leroy, A. & Bracke, M. Cellular and molecular mechanisms of metastasis as

applied to carinomatous meningitis. *J. Neurooncol.* **38,** 97–102 (1998).
25. Brastianos, P. K. *et al.* The toxicity of intrathecal bevacizumab in a rabbit model of leptomeningeal carcinomatosis. *J. Neurooncol.* **106,** 81–88 (2012).
26. Schabet, M. & Herrlinger, U. Animal models of leptomeningeal cancer. *J. Neurooncol.* **38,** 199–205 (1998).
27. Grossman, S. a. & Krabak, M. J. Leptomeningeal carcinomatosis. *Cancer Treat. Rev.* **25,** 103–119 (1999).
28. Wu, X. *et al.* Clonal selection drives genetic divergence of metastatic medulloblastoma. *Nature* **482,** 529–533 (2012).
29. Mumert, M. *et al.* Functional genomics identifies drivers of medulloblastoma dissemination. *Cancer Res.* **72,** 4944–4953 (2012).
30. Buonamici, S. *et al.* CCR7 signalling as an essential regulator of CNS infiltration in T-cell leukaemia. *Nature* **459,** 1000–4 (2009).
31. Jost, T. R. *et al.* Role of CXCR4-mediated bone marrow colonization in CNS infiltration by T cell acute lymphoblastic leukemia. *J. Leukoc. Biol.* **99,** 1077–1087 (2016).
32. Williams, M. T. S. *et al.* The ability to cross the blood-cerebrospinal fluid barrier is a generic property of acute lymphoblastic leukaemia blasts. *Blood* (2016). doi:10.1182/blood-2015-08-665034
33. Cario, G. *et al.* High Interleukin-15 Expression Characterizes Childhood Acute Lymphoblastic Leukemia With Involvement of the CNS. *J. Clin. Oncol.* **25,** 4813–4820 (2007).
34. Williams, M. T. S. *et al.* Interleukin-15 enhances cellular proliferation and upregulates CNS homing molecules in pre-B acute lymphoblastic leukemia. *Blood* **123,** 3116–27 (2014).
35. Akers, S. M., Rellick, S. L., Fortney, J. E. & Gibson, L. F. Cellular elements of the subarachnoid space promote ALL survival during chemotherapy. *Leuk. Res.* **35,** 705–711 (2011).
36. Herrlinger, U., Buchholz, R., Jachimczak, P. & Schabet, M. Intrathecal treatment of C6 glioma leptomeningeal metastasis in Wistar rats with interleukin-2. *J. Neurooncol.* **27,** 193–203 (1996).
37. Hatton, B. A. *et al.* The Smo/Smo model: Hedgehog-induced medulloblastoma with 90% incidence and leptomeningeal spread. *Cancer Res.* **68,** 1768–1776 (2008).
38. Wu, X. *et al.* Clonal selection drives genetic divergence of metastatic medulloblastoma. *Nature* **482,** 529–33 (2012).
39. Jenkins, N. C. *et al.* Genetic drivers of metastatic dissemination in sonic hedgehog medulloblastoma. *Acta Neuropathol Commun* **2,** 85 (2014).
40. Li, K. *et al.* Vascular endothelial growth factor antisense oligonucleotides inhibit leptomeningeal metastasis in vivo. *Med. Oncol.* **28,** 1116–1122 (2011).
41. Miederer, M. *et al.* Treatment of neuroblastoma meningeal carcinomatosis with intrathecal application of alpha-emitting atomic nanogenerators targeting disialo-ganglioside GD2. *Clin. Cancer Res.* **10,** 6985–92 (2004).
42. Langley, R. R. & Fidler, I. J. The biology of brain metastasis. *Clin. Chem.* **59,** 180–189 (2013).
43. Macpherson, G. R. *et al.* Retrovirus-transformed erythroleukemia cells induce central nervous system failure in a new syngeneic mouse model of meningeal leukemia. *Leuk. Res.* **36,** 369–376 (2012).

44. Boulos, N. *et al.* Chemotherapeutic agents circumvent emergence of dasatinib-resistant BCR-ABL kinase mutations in a precise mouse model of Philadelphia chromosome-positive acute lymphoblastic leukemia. *Blood* **117,** 3585–3595 (2011).
45. Williams, R. T., Roussel, M. F. & Sherr, C. J. Arf gene loss enhances oncogenicity and limits imatinib response in mouse models of Bcr-Abl-induced acute lymphoblastic leukemia. *Proc. Natl. Acad. Sci. U. S. A.* **103,** 6688–93 (2006).
46. Keller, U. B. *et al.* Myc targets Cks1 to provoke the suppression of p27Kip1, proliferation and lymphomagenesis. *EMBO J.* **26,** 2562–74 (2007).
47. Registries, N. A. A. of C. C. *Average-annual NAACCR Combined Cancer Incidence Rates for the United States, Canada and North America*. (2015). at <http://www.naaccr.org/CINA/Cina2015.v1.world.pdf>
48. Lymphoma and Leukemia Society. *Facts 2015-2016 Survivor*. (2016).
49. Longo, D. L., Hunger, S. P. & Mullighan, C. G. Acute Lymphoblastic Leukemia in Children. *N. Engl. J. Med.* **373,** 1541–1552 (2015).
50. Faderl, S., Jeha, S. & Kantarjian, H. M. The biology and therapy of adult acute lymphoblastic leukemia. *Cancer* **98,** 1337–1354 (2003).
51. Laningham, F. H. *et al.* Childhood central nervous system leukemia: Historical perspectives, current therapy, and acute neurological sequelae. *Neuroradiology* **49,** 873–888 (2007).
52. Sallan, S. E. in Adults and Children Myths and Lessons from the Adult / Pediatric Interface in Acute Lymphoblastic Leukemia. *Hematology* 128–132 (2006). doi:10.1182/asheducation-2006.1.128
53. Roberts, K. G. & Mullighan, C. G. Genomics in acute lymphoblastic leukaemia: insights and treatment implications. *Nat. Rev. Clin. Oncol.* **12,** 344–357 (2015).
54. Pui, C.-H., Relling, M. V. & Downing, J. R. Acute Lymphoblastic Leukemia. *N Engl J Med* **350,** 1535–1548 (2004).
55. Aspland, S. E., Bendall, H. H. & Murre, C. The role of E2A-PBX1 in leukemogenesis. *Oncogene* **20,** 5708–17 (2001).
56. Duque-Afonso, J. *et al.* Comparative genomics reveals multistep pathogenesis of E2A-PBX1 acute lymphoblastic leukemia. *J. Clin. Invest.* **125,** 3667–3680 (2015).
57. Zelent, A., Greaves, M. & Enver, T. Role of the TEL-AML1 fusion gene in the molecular pathogenesis of childhood acute lymphoblastic leukaemia. *Oncogene* **23,** 4275–4283 (2004).
58. Pui, C.-H. & Thiel, E. Central nervous system disease in hematologic malignancies: historical perspective and practical applications. *Semin. Oncol.* **36,** S2–S16 (2009).
59. Meyer, C. *et al.* The MLL recombinome of acute leukemias in 2013. *Leukemia* **27,** 2165–76 (2013).
60. Corral, J. *et al.* An MII-AF9 fusion gene made by homologous recombination causes acute leukemia in chimeric mice: A method to create fusion oncogenes. *Cell* **85,** 853–861 (1996).
61. Ottmann, O. G. & Wassmann, B. Acute Lymphoblastic Leukemia in Adults Treatment of Philadelphia Chromosome – Positive Acute Lymphoblastic Leukemia. *Hematology Am. Soc. Hematol. Educ. Program* (2005).
62. Kantarjian, H. M. *et al.* Identification of Risk Groups for Development of Central Nervous System Leukemia in Adults with Acute Lymphocytic Leukemia. *Blood* **72,** 1784–1789 (1988).

63. Fielding, A. K., Dc, W. & Fielding, A. K. How I treat Philadelphia chromosome − positive acute lymphoblastic leukemia How I treat How I treat Philadelphia chromosome – positive acute lymphoblastic leukemia. 3409–3417 (2013). doi:10.1182/blood-2010-01-242750
64. Salesse, S. & Verfaillie, C. M. BCR/ABL: from molecular mechanisms of leukemia induction to treatment of chronic myelogenous leukemia. *Oncogene* **21,** 8547–8559 (2002).
65. Goldman, J. M. & Melo, J. V. Chronic Myeloid Leukemia-Advances in Biology and New Approaches to Treatment. *N Engl J Med* **349,** 1451–1464 (2003).
66. Cilloni, D. & Saglio, G. Molecular pathways: BCR-ABL. *Clin. Cancer Res.* **18,** 930–937 (2012).
67. Cea, M., Cagnetta, A., Nencioni, A., Gobbi, M. & Patrone, F. New insights into biology of Chronic Myeloid Leukemia: Implications in therapy. *Curr. Cancer Drug Targets* **13,** 711–723 (2013).
68. Arlinghaus, R. & Sun, T. Signal transduction pathways in Bcr-Abl transformed cells. *Cancer Treat. Res.* **119,** 239–70 (2004).
69. Li, S., Illaria, R. L. J., Million, R. P., Daley, G. Q. & Van Etten, R. A. The P190, P210, and P230 Forms of the BCR/ABL Oncogene Induce a Similar Chronic Myeloid Leukemia-like Syndrome in Mice but Have Different Lymphoid Leukemogenic Activity. *J. Exp. Med.* **189,** 1399–1412 (1999).
70. Quinta, A. & Cortes, J. Molecular biology of bcr-abl1 – positive chronic myeloid leukemia. *Blood* **113,** 1619–1630 (2009).
71. Wigton, E. J., Thompson, S. B., Long, R. A. & Jacobelli, J. Myosin-IIA regulates leukemia engraftment and brain infiltration in a mouse model of acute lymphoblastic leukemia. **100,** 1–11 (2016).
72. Mullighan, C. G., Williams, R. T., Downing, J. R. & Sherr, C. J. Failure of CDKN2A/B (INK4A/B-ARF)-mediated tumor suppression and resistance to targeted therapy in acute lymphoblastic leukemia induced by BCR-ABL. *Genes Dev.* **22,** 1411–1415 (2008).
73. Williams, R. T. & Sherr, C. J. The INK4-ARF (CDKN2A/B) Locus in Hematopoiesis and BCR-ABL-induced Leukemias. *Cold Spring Harb. Symp. Quant. Biol.* **73,** 461–467 (2008).
74. Meacham, C. E. *et al.* A genome-scale in vivo loss-of-function screen identifies phf6 as a lineage-specific regulator of leukemia cell growth. *Genes Dev.* **29,** 483–488 (2015).
75. Wilson, J. L. *et al.* Pathway-based network modeling finds hidden genes in shRNA screen for regulators of acute lymphoblastic leukemia. *Integr. Biol.* 761–774 (2016). doi:10.1039/C6IB00040A
76. Williams, R. T., Den Besten, W. & Sherr, C. J. Cytokine-dependent imatinib resistance in mouse BCR-ABL+, Arf-null lymphoblastic leukemia. *Genes Dev.* **21,** 2283–2287 (2007).
77. Appelmann, I. *et al.* Janus kinase inhibition by ruxolitinib extends dasatinib- and dexamethasone-induced remissions in a mouse model of Ph+ ALL. *Blood* **125,** 1444–51 (2015).
78. Ramsey, L. B. *et al.* Host thiopurine methyltransferase status affects mercaptopurine antileukemic effectiveness in a murine model. *Pharmacogenet Genomics* **24,** 263–271 (2014).
79. Kular, J., Tickner, J., Chim, S. M. & Xu, J. An overview of the regulation of bone remodelling at the cellular level. *Clin. Biochem.* **45,** 863–873 (2012).

80. Charles, J. F. & Aliprantis, A. O. Osteoclasts: more than 'bone eaters'. *Trends Mol. Med.* **20,** 449–459 (2014).
81. Cappariello, A., Maurizi, A., Veeriah, V. & Teti, A. The Great Beauty of the osteoclast. *Arch. Biochem. Biophys.* **558,** 70–78 (2014).
82. Horowitz, M. C., Bothwell, A. L. M., Hesslein, D. G. T., Pflugh, D. L. & Schatz, D. G. B cells and osteoblast and osteoclast development. *Immunol. Rev.* **208,** 141–153 (2005).
83. Charles, J. F. *et al.* Inflammatory arthritis increases mouse osteoclast precursors with myeloid suppressor function. *J. Clin. Invest.* **122,** 4592–4605 (2012).
84. Kim, N., Odgren, P. R., Kim, D. K., Marks, S. C. & Choi, Y. Diverse roles of the tumor necrosis factor family member TRANCE in skeletal physiology revealed by TRANCE deficiency and partial rescue by a lymphocyte-expressed TRANCE transgene. *Proc. Natl. Acad. Sci. U.S.A.* **97,** 10905–10910 (2000).
85. Walsh, M. C. & Choi, Y. Biology of the RANKL-RANK-OPG system in immunity, bone, and beyond. *Front. Immunol.* **5,** 1–11 (2014).
86. Xiong, J. *et al.* Matrix-embedded cells control osteoclast formation. *Nat. Med.* **17,** 1235–41 (2011).
87. Hauge, E. M., Qvesel, D., Eriksen, E. F., Mosekilde, L. & Melsen, F. Cancellous bone remodeling occurs in specialized compartments lined by cells expressing osteoblastic markers. *J. Bone Miner. Res.* **16,** 1575–1582 (2001).
88. Bellido, T. Osteocyte-Driven Bone Remodeling. *Calcif. Tissue Int.* **94,** 25–34 (2014).
89. Chang, M. K. *et al.* Osteal Tissue Macrophages Are Intercalated throughout Human and Mouse Bone Lining Tissues and Regulate Osteoblast Function In Vitro and In Vivo. *J. Immunol.* **181,** 1232–1244 (2008).
90. Sinder, B. P., Pettit, A. R. & McCauley, L. K. Macrophages: Their Emerging Roles in Bone. *J. Bone Miner. Res.* **30,** 2140–2149 (2015).
91. Weitzmann, M. N. The Role of Inflammatory Cytokines, the RANKL/OPG Axis, and the Immunoskeletal Interface in Physiological Bone Turnover and Osteoporosis. *Scientifica (Cairo).* **2013,** 125705 (2013).
92. Criscitiello, C. *et al.* Crosstalk between bone niche and immune system: Osteoimmunology signaling as a potential target for cancer treatment. *Cancer Treat. Rev.* **41,** 61–68 (2015).
93. Rucci, N. Molecular pathogenesis of bone metastases in breast cancer: Proven and emerging therapeutic targets. *World J. Clin. Oncol.* **5,** 335 (2014).
94. Kang, Y. New tricks against an old foe: molecular dissection of metastasis tissue tropism in breast cancer. *Breast Dis.* **26,** 129–138 (2007).
95. Käkönen, S.-M. & Mundy, G. R. Mechanisms of osteolytic bone metastases in breast carcinoma. *Cancer* **97,** 834–9 (2003).
96. Guise, T. A. *et al.* Evidence for a causal role of parathyroid hormone-related protein in the pathogenesis of human breast cancer-mediated osteolysis. *J. Clin. Invest.* **98,** 1544–1549 (1996).
97. Fili, S., Karalaki, M. & Schaller, B. Mechanism of bone metastasis: the role of osteoprotegerin and of the host-tissue microenvironment-related survival factors. *Cancer Lett.* **283,** 10–9 (2009).
98. Juárez, P. & Guise, T. a. Tgf-Beta pathway as a therapeutic target in bone metastases. *Curr. Pharm. Des.* **16,** 1301–12 (2010).
99. Mundy, G. R. Metastasis to bone: causes, consequences and therapeutic opportunities.

*Nat. Rev. Cancer* **2,** 584–93 (2002).
100. Rahim, F. *et al.* Molecular Regulation of Bone Marrow Metastasis in Prostate and Breast Cancer. *Bone Marrow Res.* **2014,** 1–12 (2014).
101. Zhang, J. *et al.* Soluble receptor activator of nuclear factor kappaB Fc diminishes prostate cancer progression in bone. *Cancer Res.* **63,** 7883–7890 (2003).
102. Zhang, J. *et al.* Osteoprotegerin inhibits prostate cancer – induced osteoclastogenesis and prevents prostate tumor growth in the bone. **107,** 1219–1220 (2001).
103. Casimiro, S., Guise, T. a & Chirgwin, J. The critical role of the bone microenvironment in cancer metastases. *Mol. Cell. Endocrinol.* **310,** 71–81 (2009).
104. Roodman, G. D. Pathogenesis of myeloma bone disease. *Blood Cells. Mol. Dis.* **32,** 290–2 (2004).
105. Sirohi, B. & Powles, R. Multiple myeloma. *Lancet* **363,** 875–887 (2004).
106. Sezer, O. Myeloma bone disease: recent advances in biology, diagnosis, and treatment. *Oncologist* **14,** 276–83 (2009).
107. Sezer, O., Heider, U., Zavrski, I., Kühne, C. A. & Hofbauer, L. C. RANK ligand and osteoprotegerin in myeloma bone disease. *Blood* **101,** 2094–2098 (2003).
108. Standal, T. *et al.* Osteoprotegerin is bound, internalized, and degraded by multiple myeloma cells. *Blood* **100,** 3002–3007 (2002).
109. Sordillo, E. M. & Pearse, R. N. RANK-Fc: a therapeutic antagonist for RANK-L in myeloma. *Cancer* **97,** 802–812 (2003).
110. Fellmann, C. *et al.* An optimized microRNA backbone for effective single-copy RNAi. *Cell Rep.* **5,** 1704–1713 (2013).
111. Bleyer, W. A. & Poplack, D. G. Prophylaxis and treatment of leukemia in the central nervous system and other sanctuaries Bleyer, W.Archie et al. , Volume , Issue ,. *Semin. Oncol.* **12,** 131 – 148 (1985).
112. Cortes, J. Central nervous system involvement in adult acute lymphoblastic leukemia. *Hematology* **13,** 293–302 (2008).
113. Bleckmann, K. & Schrappe, M. Advances in therapy for Philadelphia-positive acute lymphoblastic leukaemia of childhood and adolescence. *Br. J. Haematol.* n/a–n/a (2016). doi:10.1111/bjh.13896
114. Ravandi, F. Managing Philadelphia chromosome-positive acute lymphoblastic leukemia: Role of tyrosine kinase inhibitors. *Clin. Lymphoma, Myeloma Leuk.* **11,** 198–203 (2011).
115. Del Principe, M. I. *et al.* Central nervous system involvement in adult acute lymphoblastic leukemia: Diagnostic tools, prophylaxis, and therapy. *Mediterr. J. Hematol. Infect. Dis.* **6,** (2014).
116. Gokbuget, N. & Hoelzer, D. Meningeosis leukaemica in adult acute lymphoblastic leukaemia. *J. Neurooncol.* **38,** 167–180 (1998).
117. Demopoulos, A. & DeAngelis, L. M. Neurologic Complications of Leukemia. *Curr. Opin. Neurol.* **15,** 691–699 (2002).
118. Nolan, C. P. & Abrey, L. E. Leptomeningeal metastases from leukemias and lymphomas. *Cancer Treat. Res.* **125,** 53–69 (2005).
119. Gleissner, B. & Chamberlain, M. Treatment of CNS dissemination in systemic lymphoma. *J. Neurooncol.* **84,** 107–117 (2007).
120. Canova, F. *et al.* Intrathecal chemotherapy in lymphomatous meningitis. *Crit. Rev. Oncol. Hematol.* **79,** 127–134 (2011).
121. Hill, Q. a. & Owen, R. G. CNS prophylaxis in lymphoma: Who to target and what therapy

to use. *Blood Rev.* **20,** 319–332 (2006).
122. Harris, A. W. *et al.* THE Emu-myc TRANSGENIC MOUSE A Model for High-incidence Spontaneous Lymphoma and Leukemia of Early B Cells Translocation of the c-myc protooncogene into or near one of the Ig loci is found in almost every case of Burkitt ' s B cell lymphoma in man and exp. *Heart* **167,** (1988).
123. Ferry, J. Burkitt's Lymphoma: Clinicopathologic Features and Differential Diagnosis. *Oncologist* 375–383 (2006). at <http://theoncologist.alphamedpress.org/content/11/4/375.short>
124. Akiyama, T. *et al.* Systemic RANK-Fc protein therapy is efficacious against primary osteosarcoma growth in a murine model via activity against osteoclasts. *J. Pharm. Pharmacol.* **62,** 470–476 (2010).
125. Manabe, N. *et al.* Connection between B lymphocyte and osteoclast differentiation pathways. *J. Immunol.* **167,** 2625–31 (2001).
126. Horowitz, M. C., Fretz, J. A. & Lorenzo, J. A. How B cells influence bone biology in health and disease. *Bone* **47,** 472–479 (2010).
127. Esposito, M. & Kang, Y. Targeting tumor–stromal interactions in bone metastasis. *Pharmacol. Ther.* **141,** 222–233 (2014).
128. Burgess, T. L. *et al.* The Ligand for Osteoprotegerin (OPGL) Directly Activates Mature Osteoclasts. *J. Cell Biol.* **145,** 527–538 (1999).
129. Kitaura, H. *et al.* Immunological reaction in TNF-alpha-mediated osteoclast formation and bone resorption in vitro and in vivo. *Clin. Dev. Immunol.* **2013,** (2013).
130. Hofbauer, L. C. *et al.* Interleukin-1B and tumor necrosis factor-a, but not interleukin-6, stimulate osteoprotegerin ligand gene expression in human osteoblastic cells. *Bone* **25,** 255–259 (1999).
131. Kobayashi, K. *et al.* Tumor Necrosis Factor a Stimulates Osteoclast Differentiation by a Mechanism Independent of the ODF/RANKL-RANK Interaction. *J. Exp. Med.* **191,** 275–285 (2000).
132. Fuller, K., Murphy, C., Kirstein, B., Fox, S. W. & Chambers, T. J. TNFa Potently Activates Osteoclasts, through a Direct Action Indepenent of and Strongly Synergistic with RANKL. *Endocrinology* **143,** 1108–1118 (2002).
133. Jinek, M. *et al.* A Programmable Dual-RNA – Guided DNA Endonuclease in Adaptive Bacterial Immunity. **337,** 816–822 (2012).
134. Jinek, M. *et al.* RNA-programmed genome editing in human cells. *Elife* **2013,** 1–9 (2013).
135. Danial, N. N. & Rothman, P. JAK-STAT signaling activated by Abl oncogenes. *Oncogene* **19,** 2523–2531 (2000).
136. Bar-Natan, M., Nelson, E. A., Xiang, M. & Frank, D. a. STAT signaling in the pathogenesis and treatment of myeloid malignancies. *Jak-Stat* **1,** 55–64 (2012).
137. Berger, A., Sexl, V., Valent, P. & Moriggl, R. Inhibition of STAT5: a therapeutic option in BCR-ABL1-driven leukemia. *Oncotarget* **5,** 9564–9576 (2014).
138. Sariban, E., Edwards, C., Janus, B. & Magrath, I. Central nervous system involvement in American Burkitt's lymphoma. *J. Clin. Oncol.* **1,** 677–681 (1983).
139. Seymour, J. F. & Kantarjian, H. M. Hypercalcemia in acute lymphoblastic leukemia. *Leuk Res* **18,** 231–232 (1994).
140. Sinigaglia, R. *et al.* Musculoskeletal manifestations in pediatric acute leukemia. *J. Pediatr. Orthop.* **28,** 20–28 (2008).
141. Kuroda, I. *et al.* BCR-ABL regulates death receptor expression for TNF-related apoptosis-

inducing ligand (TRAIL) in Philadelphia chromosome-positive leukemia. *Oncogene* **32,** 1670–81 (2013).
142. Wang, J., Rouse, C., Jasper, J. S. & Pendergast, A. M. ABL kinases promote breast cancer osteolytic metastasis by modulating tumor-bone interactions through TAZ and STAT5 signaling. **9,** 1–14 (2016).
143. Hoelbl, A. *et al.* Stat5 is indispensable for the maintenance of Bcr/Abl-positive leukaemia. *EMBO Mol. Med.* **2,** 98–110 (2010).